Introduction to Quantum Monte Carlo Methods Applied to the Electron Gas

D. M. Ceperley

Physics Department and NCSA, University of Illinois Urbana-Champaign, Urbana, IL, USA

1. – Introduction

In these lectures, I will briefly review some of the Quantum Monte Carlo (QMC) methods that have been used to calculate properties of the "electron gas" and review properties that have been computed with these methods. (Note that this article is a mosaic of previously published works on this subject with very little genuinely new results. It is hoped that this collection will prove useful.) For the electron gas, QMC has been very useful in providing exact results, or at least exact constraints, on its properties, though with some remaining approximations. Fermion statistics remain a challenge to the practitioner of quantum simulation techniques. Nonetheless, the results are in many cases more accurate than those from the other quantum many-body methods, particularly for the case of strong correlation. There has been significant progress in the last decade in improving the methods. We will describe these improved methods.

The ground state properties of the electron gas are entirely determined by the density parameter $r_s = a/a_0$ where in 3D, $4\pi\rho a^3/3 = 1$ and a_0 is the bohr radius, possibly changed from its vacuum value by band effects. In effective Rydbergs, the Hamiltonian is :

$$H = -\frac{1}{r_s^2}\sum_{i=1}^{N}\nabla_i^2 + \frac{2}{r_s}\sum_{i<j}\frac{1}{|\mathbf{r}_i - \mathbf{r}_j|} + const. \tag{1}$$

Note that the kinetic energy scales as $1/r_s^2$ and the potential energy scales as $1/r_s$ so that for small r_s (high electronic density), the kinetic energy dominates, and the electrons

behave like ideal gas; in the limit of large r_s, the potential energy dominates and the electrons crystallize into a Wigner crystal[1].

First few words on notation. I will always assume that the system is a non-relativistic collection of N particles with $\lambda = \hbar^2/2m$. I will stick to the first quantized notation in the canonical ensemble. A boson wave function is then totally symmetrical under particle exchange and a fermion function is antisymmetrical. The symbol R refers to the $3N$ vector of particle coordinates, σ to the N spin coordinates, and (r_i, σ_i) to the 3 spatial and 1 spin coordinate of particle i. The permutation operator acting on particle labels is denoted PR. Sometimes I will refer to the exact eigenfunctions and eigenvalues of the Hamiltonian: $(\phi_\alpha(R), E_\alpha)$. A known (computable) trial wave function will be denoted $\Psi(R)$. The symbol $\int$ will imply an integral over the full $3N$ dimensional configuration space of the particles, and possibly a sum over spin variables.

We first discuss the QMC methods at T=0, then the obtained results, then the finite temperature methods and corresponding results. We restrict ourselves to the homogeneous electron gas. There are many applications to inhomogeneous systems[3] but we do not have space to consider them.

2. – Variational Monte Carlo

2˙1. *Random Walks.* – Monte Carlo methods for many-body systems are exclusively examples of Markov processes or random walks. Let us briefly review their basic concepts. Let $\mathcal{S}$ be a state space and let $(s_0, s_1, \ldots)$ be a random walk in that space. The choice of the state space will vary depending on the method, but for now, let s_i represent the $3N$ coordinates of all the particles. In the simplest Markov process, there is a constant transition probability for generating state b given that the walk is presently in state a, which we will denote P_{ba}. The transition probability, or moving rule, generates the walk. Under very general conditions [2], the asymptotic probability distribution of the walk converges exponentially fast to a unique distribution:

$$\mathcal{P}(s_n) \to \Pi(s_n). \tag{2}$$

In projector Monte Carlo, the transition rules are set up so that the asymptotic population is the ground state wave function for a given Hamiltonian. In the Metropolis [4, 5] rejection method, moving the particles is a two step process; first one samples a trial position, (state a'), from a transition probability $T_{a'a}$, then this trial move is either accepted (i.e. $b = a'$) or rejected (i.e. $b = a$) with a probability given by:

$$min\left[1, \frac{\Pi_{a'} T_{aa'}}{\Pi_a T_{a'a}}\right]. \tag{3}$$

The acceptance probability has been chosen to satisfy the detailed balance relation which implies that its asymptotic probability will converge to Π_a independent of the transition rules $T_{aa'}$. The rate of convergence or the efficiency of the walk in sampling state space

is determined by the transition rules and the distribution to be sampled. The rejection method is appropriate when one wants to sample a known, computable function. If one had an exact analytic expression for the many-body wave function, it would then be straightforward to use this method to determine quantum expectation values in that state. However, such is not the case, and one is forced to resort to either more complicated, or more approximate methods.

2˙2. *The Variational Method.* – The variational Monte Carlo method was first used by McMillan [6] to calculate the ground state properties of liquid ^4He and then generalized to fermion systems by Ceperley et. al[7]. The variational theorem says that for Ψ a proper trial function, the variational energy of the trial function is an upper bound to the exact ground state energy:

$$E_V = \frac{\int \Psi^*(R)\mathcal{H}\Psi(R)}{\int \Psi^*(R)\Psi(R)} \geq E_0. \tag{4}$$

The trial function must satisfy the following conditions:

1. Ψ has the proper symmetry: $\Psi(R) = (-1)^P\Psi(PR)$ for fermions and the right behavior at the periodic boundaries.
2. $\mathcal{H}\Psi$ is well defined everywhere which means that both Ψ and $\nabla\Psi$ must be continuous wherever the potential is finite.
3. The integrals $\int \Psi^2$, $\int \Psi^2\mathcal{H}\Psi$, and $\int(\Psi\mathcal{H})^2$ should exist. The last integral is only required to exist for a Monte Carlo evaluation of the integrals. If it does not exist the statistical error of the energy will be infinite.

In the continuum, it is important to show analytically that properties 2 and 3 hold everywhere, particularly at the edges of the periodic box and when two particles approach each other. Otherwise either the upper bound property is not guaranteed or the Monte Carlo error estimates are not valid.

The variational method is then quite simple. Use the Metropolis algorithm to sample the square of the modulus of the wave function:

$$\Pi(R) = \frac{\mid \Psi(R) \mid^2}{\int \mid \Psi(R) \mid^2}. \tag{5}$$

(Note that this may also include spin degrees of freedom.) Then the variational energy is simply the average value of the *local energy* over this distribution,

$$E_V = \int \Pi(R)E_L(R) = \langle E_L(R)\rangle \tag{6}$$

where the local energy of Ψ is defined as:

$$E_L(R) = \Re\{\Psi^{-1}\mathcal{H}\Psi(R)\}. \tag{7}$$

Variational Monte Carlo(VMC) has a very important zero variance property : as the trial function approaches an exact eigenfunction, $\Psi \rightarrow \phi_\alpha$, the local energy approaches the eigenvalue everywhere, $E_L(R) \rightarrow E_\alpha$, and the Monte Carlo estimate of the variational energy converges more rapidly with the number of steps in the random walk. Of course, in this limit the upper bound is also converging to the true energy. It is because of the zero variance property that Quantum Monte Carlo calculations of energies can be much more precise than Monte Carlo calculations of classical systems. Fluctuations (statistical errors) are only due to inaccuracies in the trial function.

2˙3. *The Pair Product Trial Function.* – The pair product trial function is the simplest generalization of the Slater determinant and the ubiquitous form for the trial function in variational Monte Carlo:

$$\Psi(R,\sigma) = exp[-\sum_{i<j} u(r_{ij})] det[\theta_k(r_i,\sigma_i], \tag{8}$$

where $\theta_k(r,\sigma)$ is the k^{th} spin-orbital and $\theta_k(r_i,\sigma_i)$, the Slater matrix, and $u(r)$ is the "pseudopotential" or pair correlation factor. This function also goes by the name of a Jastrow[8] wave function, although Bijl[9] much earlier described the motivation for its use in liquid ^{4}He. Closely related forms are the Gutzwiller function for a lattice, or the Laughlin function in the fractional quantum hall effect. Both $u(r)$ and $\theta_k(r,\sigma)$ are, in principle, determined by minimizing the variational energy.

2˙4. *Details.* – I will only mention a few details concerning VMC. First, how do the particles move? In the continuum it best to move the electrons one at a time, by adding a random vector to the electron's coordinate, where the vector is either uniform inside of a cube centered about the old coordinate, or is a normally distributed random vector, as we will discuss below with DMC. Assuming the first kind of move for the i^{th} particle, the trial move is accepted with probability:

$$\mid \Psi(R')/\Psi(R) \mid^2 = exp[-2\sum_{j\neq i}(u(r_i'-r_j)-u(r_i-r_j))] \mid \sum_k \theta_k(r_i')C_{ki} \mid^2, \tag{9}$$

where the matrix, C, is the transposed inverse to the Slater matrix. The evaluation of a general determinant takes $O(N^3)$ operations. The evaluation of the fermion part of the acceptance ratio will take $O(N)$ operations if C is kept up to date. If a move is accepted, C needs to be updated [7] which takes $O(N^2)$ operations. Hence, to attempt moves for all N particles (a pass) takes $O(N^3)$ operations.

The local energy, needed to evaluate the variational energy, is calculated by applying the Hamiltonian to the trial function:

$$E_L(R) = V(R) + \lambda \sum_i [\nabla_i^2 U - \sum_k \nabla_i^2 \theta_k(r_i) C_{ki} - G_i^2] \tag{10}$$

where $G_i = -\nabla_i U + \sum_k \nabla_i \theta_k(r_i) C_{ki}$ and $U = \sum u(r_{ij})$. Thus, the inverse matrix is also needed to determine the local energy. Very often the orbitals are taken to be exact solutions to some model problem, in which case the term, $\nabla_i^2 \theta_k(r_i)$, will simplify.

2˙5. *Optimization of Trial Functions*. – Optimization of the parameters in a trial function is crucial for the success of the variational method and important for the Projector Monte Carlo method. There are several possibilities of the quantity to optimize.

- The variational energy: E_V. Clearly one minimizes E_V if the object of the calculation is to find the least upper bound to the energy. There are some general arguments suggesting that the trial function with the lowest variational energy will maximize the efficiency of Projector Monte Carlo [10].
- The dispersion of the local energy of the *variance* :$\int [(\mathcal{H} - E_V)\Psi]^2$. If we assume that every step on a QMC calculation is statistically uncorrelated with the others, the dispersion is proportional to the variance of the calculation. The minimization of the dispersion is statistically more robust than the variational energy because it is a positive definite quantity.
- The overlap with the exact wave function: $\int \Psi\phi$. This is equivalent to finding the trial function which is closest to the exact wave function in the least squares sense. This is the preferred quantity to optimize if you want to calculate correlation functions, not just ground state energies. Optimization of the overlap will involve a Projector Monte Carlo calculation to determine it, a more computer intensive step.

We will now review the analytic properties of the optimal pseudopotential. Let us assume that the spin-orbits come from an exact solution for some model potential. Consider bringing 2 particles together and let us examine the dominant terms in the local energy. In a good trial function, the singularities in the kinetic energy must cancel those in the potential. The singular parts of local energy will have the form:

$$E_L(R) = v(r) + 2\lambda\nabla^2 u(r) - 2\lambda(\nabla u(r))^2 + \dots \tag{11}$$

where r is the distance separating the particles. An intuitive result emerges: $e^{-u(r)}$ will equal the solution to the 2-body Schrödinger equation. For the Coulomb potential this equation gives the "cusp condition", the value of the derivative of the pseudopotential at the origin:

$$\left.\frac{du}{dr}\right|_0 = -\frac{e^2}{2\lambda(D-1)}. \tag{12}$$

Even more important is the large r behavior of the optimal $u(r)$ where a description in terms of collective coordinates (the plasmons) is appropriate. This is important because the long-wavelength modes are important for the low energy response properties and

they are also the slowest to converge in QMC. In k-space, the variational energy can be written as:

$$E_V = E_F + \sum_k (v_k - \lambda k^2 u_k)(S_k - 1) \tag{13}$$

where E_F is the fermion energy in the absence of correlation, v_k and u_k are the fourier transforms of $v(r)$ and $u(r)$ and S_k is the static structure factor for a given $u(r)$. Minimizing E_V with respect to u_k and making the RPA assumption of how S_k depends on u_k: $S_k^{-1} = S_{0k}^{-1} + 2\rho u_k$ where ρ is the particle density and S_{0k} is the structure factor for uncorrelated fermions, we obtain[11] the "Gaskell" or RPA form[12] at long wavelengths:

$$2\rho u_k = -\frac{1}{S_{0k}} + [\frac{1}{S_{0k}} + \frac{2\rho v_k}{\lambda k^2}]^{1/2}. \tag{14}$$

Here the fourier transform of the pair potential is $v_k = 2\pi(D-1)e^2 k^{D-1}$. This gives the following behavior of the 2DEG and 3DEG pseudopotential: $\lim_{r\to\infty} u(r) \propto r^{-(D-1)/2}$. Not only the power, but also the coefficient is exactly correct. This Gaskell form is optimal at both long distances and at short distances, but not necessarily in between. For the 2DEG and 3DEG, this parameter-free form can hardly be improved by assuming an arbitrary function and is basically correct even in the strongly correlated regime, though the RPA assumption on which it is based, is not.

This raises a very important point which we will not have space to go into. The Coulomb potential is long-ranged, so that treatment of a finite system in periodic boundary conditions requires an assumption about how to handle the part of the potential sticking out of the box. For high accuracy results and physically correct properties in the long wavelength limit, the Ewald image method[13, 11] is needed to represent the correct long-range behavior of the potential and the trial function. The optimal pseudopotentials are always long-ranged in the sense that correlation will extend beyond the simulation box. The ground state energy is not very much affected by this tail in the wave function, but response function, such as the dielectric function or static structure factor are crucially dependent on using the correct long-range properties. In order to maintain the upper bound property, the correlation function must be properly periodic in the simulation cell. See ref. [14] for an efficient way to treat numerically any long-range function within periodic boundary conditions.

At intermediate distances or for highly correlated or complex systems, a purely Monte Carlo optimization method may be needed. The simplest such method consists of running independent VMC runs with a variety of different variational parameters, fitting the results energies with a quadratic form, doing more calculations at the predicted minimum, *etc.* , until convergence in parameter space is attained. The difficulty is that close to the minimum the independent statistical errors will mask the variation with respect to the trial function parameters. The derivative of the variational energy with respect to trial function parameters is very poorly calculated. It is difficult to optimize by hand

functions involving more than 3 variational parameters. A correlated sampling method, known as reweighting[15, 7] solves this problem.

2˙6. *The spin-orbits: Crystal vs. Liquid.* – The description of the trial function in the previous section did not discuss the spin-orbits that enter into the slater determinant nor how we will distinguish between the liquid and crystal. In a homogenous liquid, plane waves are a self-consistent solution to the Hartree-Fock equations with the occupied states chosen to have an energy less than the Fermi level. It is known, however, that this solution is unstable to broken symmetry states, in particular to ferromagnetic solutions and to spin density waves. Attempts to use such orbitals in conjunction with a Jastrow factor have generally led to higher energies. We will discuss the ferromagnetic case where one does find a deviation from the non-interacting spin-orbits.

At very strong correlations, Wigner showed the system must crystallize. However, the plane wave determinant even with a Jastrow correlation factor, does not provide a good description of the crystal. At the VMC level, the broken spatial symmetry of the crystal needs to be put in by hand. That is typically done by making spin-orbitals which are localized on lattice sites. It has been found the spherical Gaussian work as well as more complicated functions for the 2DEG and 3DEG:

$$\theta_i(\mathbf{r}) = \exp(-C(\mathbf{r} - \mathbf{Z}_i)^2) \tag{15}$$

where C is a variational parameter and $\mathbf{Z}_i$ is a set of lattice sites. To minimize the potential energy these are usually taken as a triangular lattice in 2D and a bcc lattice in 3D. Since the bcc lattice is bipartite, one can then place the two species of spin on the two sublattices. The triangular lattice cannot be handled this way. We will discuss the spin properties of the Wigner crystal at the end of these notes.

It is found that these spin-orbits are very successful[32] for the perfect crystal, even though the broken symmetry is put in by hand. Note that the long range properties of the optimal Jastrow factor are slightly modified[11]. "Shadow" trial functions, where one introduces a set of shadow particles[16], can spontaneously break the symmetry, and provide a better description of defective crystals, or near melting, however, treatment of Fermi statistics with those functions is numerically difficult.

2˙7. *Beyond the pair-product trial function.* – There is important progress in finding trial functions significantly more accurate than the pair product, Slater-Jastrow function.

- One can replace the spin-orbitals with pairing functions. For example, if the particles are paired in a spin singlet state one obtains a determinant of the form:

$$det[\chi_s(r_i \uparrow, r_j \downarrow)] \tag{16}$$

  or if the particles are paired in a spin triplet:

$$\mathcal{A} \prod_{i=1}^{N/2} \chi_p(r_{2i}, r_{2i-1}) \tag{17}$$

where $\mathcal{A}$ is an antisymmetrizer. Bouchaud and Lhuiller [17] have pointed out the this object is a pfaffian and hence one can use the theorem that the square of a pfaffian is a determinant to sample it with VMC. To date, no one has succeeded in getting lower energy with this trial function than the SJ energy.

- The dominant term missing in the trial function for bosonic system is a three body term with the functional form of a squared force:

$$U_3(R) = -\sum_i [\sum_j \xi(r_{ij}) \vec{r_{ij}}]^2. \tag{18}$$

The form, a square, makes it particularly rapid to compute. It is not much slower than a 2 body function. This term is particularly important at strong correlation, at large r_s[18, 19].

- The dominant correction for the pair-product trial function is to modify the spin-orbitals to include backflow correlations. The particle coordinates in the Slater determinants become 'quasi-particle' coordinates:

$$det[\theta_k(\vec{x}_i, \sigma_i], \tag{19}$$

where the "quasi-particle" coordinates are defined by: $\vec{x}_i = \vec{r}_i + \sum_j \eta(r_{ij})\vec{r}_{ij}$. Backflow is needed to satisfy local current conservation. The $\eta(r)$ function is similar to the "pseudopotential" however it decays more quickly, as r^{-3} in 3D. A good approximation to its form is discussed in [21]. Because this affects the orbitals, it also affects the nodes (or phases) of the many-body trial function. Thus it is extremely important in conjunction with the fixed-node approach.

Table 1 gives VMC energies for the 3DEG with SJ trial function and with improved 3 body backflow. There has been recent progress[21] in finding analytic properties of the backflow functions. Such analytic forms are quite accurate for $r_s \leq 20$ and are shown in figs. 1-2.

2˙8. *Finite size effects.* – The dependence of the energy on the number of electrons is the largest systematic error in quantum Monte Carlo calculations but fortunately it can be minimized by several methods. The largest effect in fermion systems comes from the kinetic energy, arising from the erratic filling of the shells in k-space. If one uses periodic boundary conditions for the wavefunction the resulting energy per electron for free particles is shown in fig. 3

Though PBC with Fermi Liquid Theory (FLT) corrections[11] are adequate for unpolarized and fully polarized systems, the precision is limited for intermediate polarizations. To estimate finite size effects within FLT, one must perform accurate DMC simulations for widely varying system sizes. For example, in Ortiz et al.[22] calculation of the electron gas, the simulation size varied from $725 \leq N \leq 1450$. Within DMC it is very time-consuming to ensure uniform accuracy independent of particle number, so that

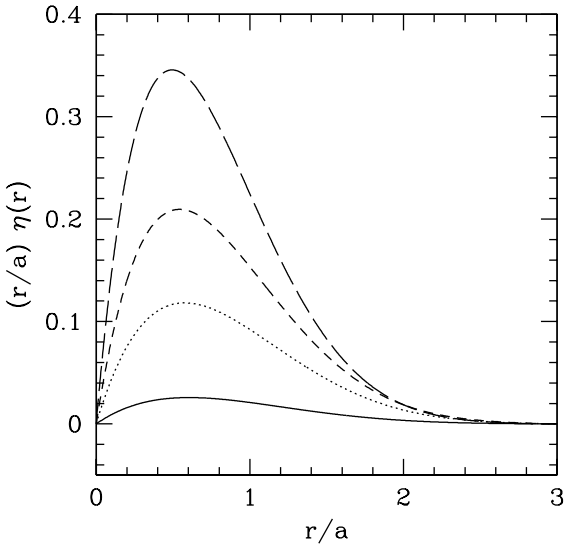

Fig. 1. – The change in the quasiparticle coordinate $r\eta(r)$ (analytic backflow) caused by an electron a distance r away in the 3D electron gas. Graphed is only the short range part of η with $N = 54$. The four figures are for $r_s = 1, 5, 10, 20$ from the bottom to the top of the figure.

r_s	wavefunction	E_v	σ^2	E_{DMC}
1	SJ	1.0669 (6)	1.15 (2)	1.0619 (4)
	BF-A	1.0611 (2)	0.029 (1)	1.0597 (1)
5	SJ	-0.15558 (7)	0.0023(1)	-0.15734 (3)
	BF-A	-0.15762 (1)	0.00061 (1)	-0.15810 (1)
10	SJ	-0.10745 (2)	0.00039 (.5)	-0.10849 (2)
	BF-A	-0.10843 (2)	0.00017 (1)	-0.10888 (1)
20	SJ	-0.06333 (1)	0.000064 (1)	-0.06388 (1)
	BF-A	-0.06372 (2)	0.000045 (2)	-0.06408 (1)

Table I. – *Energies and variances for the 3D electron gas with $N = 54$ unpolarized electrons in Rydbergs/electron. SJ means a Slater determinant of plane waves times an optimized Jastrow factor. BF-A are the results using the RPA Jastrow, together with the analytical backflow formula. σ^2 is the variance of the local energy per electron.*

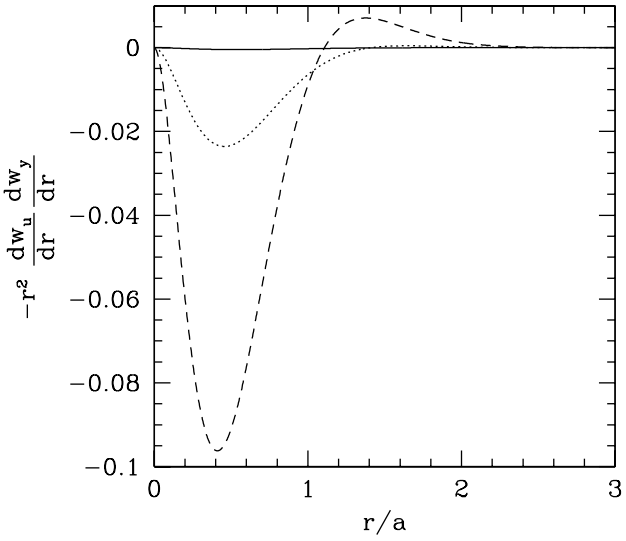

Fig. 2. – The three-body contribution to the logarithm of the wavefunction due to three electrons in the 3D electron gas. This is just the short range parts of $w(r)$ for $N = 54$. The solid line, for $r_s = 1$, is close to zero (maximum magnitude of 3×10^{-4}). The dotted line and dashed lines are for $r_s = 5, 10$.

one typically determines size effects within VMC, using the more approximate SJ trial functions.

Within periodic boundary conditions (PBC), the phase picked up by the wavefunction as a particle makes a circuit across the unit cell, is arbitrary. General boundary conditions are:

$$\Psi(\mathbf{r}_1 + L, \mathbf{r}_2, \ldots) = e^{i\theta}\Psi(\mathbf{r}_1, \mathbf{r}_2, \ldots) \tag{20}$$

where L is a lattice vector of the supercell. If the twist angle θ is averaged over, most single-particle finite-size effects arising from shell effects in filling the plane wave orbitals, are eliminated[23] as can be seen in the figure. If one uses grand canonical simulations, all single particle kinetic finite size effects are eliminated. TA boundary conditions allow a much better way to estimate energies in the thermodynamic limit of partially polarized fermi liquids since the number of electrons can be held fixed as the spin polarization varies.

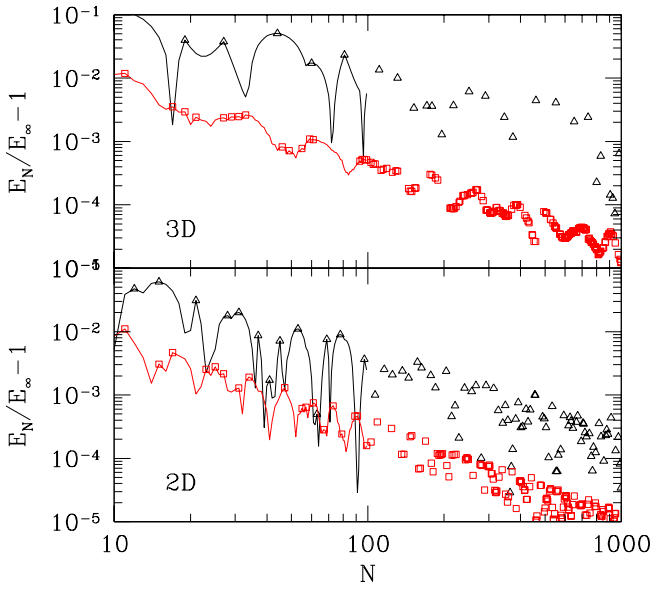

Fig. 3. – Relative error of the energy versus number of particles with PBC and TABC in 2D and 3D. The points shown are only those where the relative error has a local maximum. Curves are shown only for $N < 100$.

The potential effects are more difficult since they are due to pair interaction effects. To correct this, one fits the energies versus N using the expansion:

$$E_N = E_\infty + \frac{a_1}{N} + \frac{a_2}{N^2} + \dots . \tag{21}$$

Results for several different sizes are necessary to use this formula, though we have made some recent progress with analytic corrections within the GCE.

2˙9. *Problems with Variational Methods.* – The variational method is very powerful, and intuitively pleasing. One posits a form of the trial function and then obtains an upper bound. In contrast to other theoretical methods, no further essential approximations need to be made and there are no restrictions on the trial function except that it be computable in a reasonable amount of time. To be sure, the numerical work has to be done very carefully which means that convergence of the random walk has to be tested and dependence on system size needs to be understood. To motivate the methods to

be described in the next section, let me list some of the intrinsic problems with the variational method.

- The variational method favors simple states over more complicated states. One of the main uses of simulations is to determine when and if a zero-temperature phase transition will occur. As an example, consider the liquid-solid transition at zero temperature. The solid wave function is simpler than the liquid wave function because in the solid the particles are localized so that the phase space that the atoms explore is much reduced. This means that if you compare liquid and solid variational energies for the same type of trial function, (e.g. a pair product form) the solid energy will be closer to the exact result than the liquid and hence the transition density will be systematically lower than the experimental value. VMC calculations in the e-gas show this effect[11]. Another example; the wave function for fully polarized electron gas is simpler than for unpolarized system so that the spin susceptibility computed at the pair product level has the wrong sign.
- The optimization of trial functions for many-body systems is very time consuming, particularly for complex trial functions. This allows an element of human bias; the optimization is stopped when the expected result is obtained.
- The variational energy is insensitive to long range order. The energy is dominated by the local order (nearest neighbor correlation functions). If one is trying to compare the variational energy of a trial functions with and without long range order, it is extremely important that both functions have the same short-range flexibility and both trial functions are equally optimized locally. Only if this is done, can one have any hope of saying anything about the long range order. The error in the variational energy is second order in the trial function, while any other property will be first order. Thus variational energies can be quite accurate while correlation function completely incorrect.
- You almost always get out what is put in. Suppose the spin-orbitals have a Fermi surface. Then the momentum distribution of the pair product trial function will also have a Fermi surface although it will be renormalized. This does not imply that the true wave function has a sharp Fermi surface. Only if localized spin-orbitals are used will a gap appear.

3. – Diffusion Monte Carlo

Now I will turn to a more powerful method than VMC where a function of the Hamiltonian projects out the the ground state, hence the name, projector Monte Carlo. For simplicity I will only discuss Diffusion Monte Carlo although most of what I say carries over immediately to other projectors. A sequence of trial functions is defined by applying the projector, $G(R, R')$:

$$\psi_{n+1}(R) = e^{-\tau(\mathcal{H}-E_T)}\psi_n(R) = \int dR' G(R, R')\psi_n(R') \tag{22}$$

with the initial condition: $\psi_0(R) = \Psi(R)$. The effect on the trial function of the Green's function is seen by expanding the trial function in the exact eigenfunctions of the Hamiltonian:

$$\psi_n(R) = \sum_\alpha \phi_\alpha(R) < \phi_\alpha|\Psi > e^{-n\tau(E_\alpha - E_T)}. \tag{23}$$

The Green's function will project out the state of lowest energy having a non-zero overlap with the initial trial function.

$$\lim_{n\to\infty} \psi_n(R) = \phi_0(R) < \phi_0|\Psi > e^{-n\tau(E_0 - E_T)}. \tag{24}$$

The role of the trial energy is to keep the overall normalization of ψ_n fixed, which implies $E_T \approx E_0$. The time step, τ, controls the rate of convergence to the ground state. It is controlled by the needed to determine the projecting function.

For many-body systems, the trial function and the Green's function are sampled. For the moment let us discuss the case where Ψ is non-negative, the boson case. In the limit that the time step approaches zero, a coordinate space representation of the Green's function is:

$$< R|e^{-\tau(\mathcal{H} - E_T)}|R' >= (4\pi\lambda\tau)^{-3N/2} e^{-\frac{(R-R')^2}{4\lambda\tau}} e^{-\tau(V(R) - E_T)} \; + \; O(\tau^2) \tag{25}$$

The iteration equation, eq. 25, has a simple interpretation in terms of branching random walks since the first factor is the Green's function for diffusion and the second is multiplication of the distribution by a positive scalar.

An ensemble of configurations is constructed with a Metropolis sampling procedure for $\Psi(R)$. This is called the zeroth generation, i.e. $n = 0$, and the number of configurations is the population of the zeroth generation, P_0. Points in the next generation are constructed by sampling the Gaussian distribution in eq. (25) and then branching. The number of copies of R' in the next generation is the integer part of $u + \exp[-\tau(V(R) - E_T)]$ where u is a uniform random number in $(0, 1)$. If the potential energy is less than the ground state energy, duplicate copies of the configuration are generated. In future generations, these walks propagate independently of each other. In places of high potential energy, random walks are terminated.

The above procedure, depicted in fig. (2), is a Markov process where the state of the walk in the nth generation is $\{P_n; R_1, R_2, \ldots R_{P_n}\}$. Hence it has a unique stationary distribution, constructed to be the ground state wave function. The number of walkers fluctuates from step to step. The trial energy, E_T, must be adjusted to keep the population within computationally acceptable limits.

3˙1. *Importance Sampling.* – The above scheme, first suggested by Fermi, was actually tried out in the first days of computing some fifty years ago[24]. But it fails on many-body systems because the potential is unbounded. For example, a coulomb potential can go to both positive and negative infinity. Even with a bounded potential

the method becomes very inefficient as the number of particles increases. But there is a very simple cure discovered by Kalos[25] for GFMC but equally applicable to any projector method. Importance sampling multiplies the underlying probability distribution by a known, approximate solution. Multiply eq. (22) by Ψ, the trial function, and let $f_n(R) = \Psi(R)\psi_n(R)$. Then:

$$f_{n+1} = \Psi e^{-\tau(\mathcal{H}-E_T)}\psi_n = \int dR' \tilde{G}(R,R') f_n(R') \tag{26}$$

where $\tilde{G}(R,R') = \Psi^{-1} e^{-\tau(\mathcal{H}-E_T)}\Psi$ is the importance-sampled Green's function and the initial conditions are $f_0(R) = \Psi^2(R)$. It is easily shown by differentiating $\tilde{G}$ with respect to τ that it satisfies the evolution equation:

$$-\frac{\partial \tilde{G}(R,R_0;\tau)}{\partial \tau} = -\sum_i \lambda_i \nabla_i [\nabla_i \tilde{G} + 2\tilde{G}\nabla_i \ln(\Psi(R))] + [E_L(R) - E_T]\tilde{G} \tag{27}$$

where E_L is the local-energy defined in eq. (7). The first three terms on the right-hand side correspond to diffusion, drifting and branching. As the trial function approaches the exact eigenfunction, the branching factor approaches unity; thus a sufficiently good trial function can control the branching.

The importance sampled DMC algorithm[26, 51] is:

1. The ensemble is initialized with a VMC sample from $|\Psi(R)|^2(R)$
2. The points in the configuration are advanced in time as:

$$R_{n+1} = R_n + \chi + \lambda\tau\nabla \ln(|\Psi(R_n)|^2). \tag{28}$$

   where χ is a normally distributed random vector with variance $2\lambda\tau$ and zero mean.

3. The number of copies of each configuration is the integer part of

$$exp(-\tau(E_L(R_n) - E_T)) + u \tag{29}$$

   where u is a uniformly distributed random number in $(0,1)$.

4. The energy is calculated as the average value of the local energy: $E_0 = \langle E_L(R_n)\rangle$.
5. The trial energy is periodically adjusted to keep the population stable.
6. To obtain ground state expectations of quantities other than the energy, (e.g. the potential energy) one must correct the average over the DMC walk, the so-called "mixed estimator", $V_{mix} =< \phi_0|V|\Psi >$ with using the variational estimator[15].

$$< \phi_0|V|\phi_0 >= 2 < \phi_0|V|\Psi > - < \Psi|V|\Psi > + O([\phi_0 - \Psi]^2) \tag{30}$$

   If the mixed estimator equals the variational estimator then the trial function has maximum overlap with the ground state.

3˙2. *The Fixed-Node Method.* – We have not discussed at all the problem posed by fermi statistics for projector Monte Carlo. Consider the difficulty in implementing the non-importance sampled algorithm: the initial condition is not a probability distribution since a fermion trial function will have positive and negative pieces. Hence, we must use the initial sign of the wave function as a weight for the random walk. That leads to an exact, but slowly converging algorithm, that we will discuss it in the next subsection.

Now suppose we use an antisymmetric trial function in the importance-sampled algorithm. The initial distribution is positive, but the Green's function, $\tilde{G}(R, R')$ can be negative if a step changes the sign of Ψ. Thereafter a minus sign will be attached to the walk which will lead to a growing statistical variance for all estimators. But there is a simple way to avoid the sign: forbid moves in which the sign of the trial function changes. This is the fixed-node (FN) approximation.

In a diffusion process, forbidding node crossings puts a zero boundary condition on the evolution equation for the probability. This solves the wave equation with the boundary conditions that it vanish wherever the trial function vanishes. One can easily demonstrate that the resulting energy will be an upper bound to the exact ground state energy[27]; the best possible upper bound with the given boundary conditions. With the FN method, we do not necessarily have the exact fermion energy, but the results are much superior to those of VMC. No longer do we have to optimize two-body correlation factors, three-body terms etc., since the nodes of the trial function are unchanged by those terms. One is exactly solving the wave equation inside the fixed-nodal regions, but there is a mismatch of the derivative of the solution across the boundary. The nodes have an unequal "fermion" pressure on the two sides unless the nodes are exact. Where comparison has been done between the VMC energy, the FN-DMC energy and the exact answer, one generally finds that the systematic error in the FN calculation is three to ten times smaller than it would be for a well optimized VMC energy.

The nodes obviously play a very important role since, as we have seen, if the nodes were exactly known, the many-fermion system could be treated by Monte Carlo methods without approximation. The ground state wave function can be chosen real in the absence of magnetic fields; the nodes are the set of points where $\phi(R) = 0$. Since this is a single equation, the nodes are in general a $3N - 1$ dimensional hypersurface. When any two particles with the same spin are at the same location the wave function vanishes. These coincident planes, with $r_i = r_j$ are $3N - 3$ dimensional hypersurfaces. In 3D space they do not exhaust the nodes, but are a sort of scaffolding. The situation is very different in $1D$ where the set of nodes is usually equal to the set of coincident hyperplanes. Fermions in $1D$ are equivalent to $1D$ bosons with a no-exchange rule.

Nodal volumes of ground state wave functions possess a tiling property[28]. To define this property first pick a point, R_0, which does not lie on the nodes. Consider the set of points which can be reached from R_0 by a continuous path with $\phi(R) \neq 0$. This is the volume in phase space accessible to a fixed-node random walk starting at R_0. Now consider mapping this volume with the permutation operator (only permute like spins), *i.e.* relabel the particles. The tiling theorem says that this procedure completely fills phase space, except, of course, for the nodes. Thus one does not have to worry about

where the random walk started; all starting places are equivalent. This theorem applies for any fermion wave function which is the ground state for some local Hamiltonian and it can be proved by a simple variational argument. Excited states, or arbitrary antisymmetric functions need not have the tiling property. More extensive discussion of fermion nodes and some pictures of cross-sections of free particle nodes are given in ref. [28].

3˙3. *Fixed phase method.* – We can generalize the fixed-node method to complex trial functions[43]. Let us take an arbitrary complex wave function and divide its logarithm into its real and imaginary parts: $\phi(R) = exp(-M(R)+iS(R))$. For a given fixed-phase, let us minimize the variational energy with respect to M. We are left with an effective Hamiltonian with an additional repulsive term in the potential energy coming from the phase of the trial function:

$$\Delta\mathcal{H} = -\lambda \sum_{i}^{N} [\nabla S(R)]^2 \tag{31}$$

with $S(R)$ the phase of the trial function. Then this equation can be solved with the bosonic DMC method described above. We do not solve the full Schrödinger equation since we have not optimized the energy with respect to the phase. That is we have an error in the continuity equation. In contrast to the method for real wavefunctions, there is no barrier to the diffusion (no nodes), just regions where the phase is rapidly varying, leading to a large (but not infinite) effective potential.

3˙4. *Exact Fermion Methods.* – As accurate as the FN method might be, it is still unsatisfactory since one does not know how the assumed nodal structure will affect the final result. One might guess that long-range properties, such as the existence or non-existence of a fermi surface will be determined by the assumed nodes. The FN algorithm is only improving the bosonic correlations of the trial function, not the fermion features. There are some fairly simple ways of improving on the FN method, but their use is limited.

The transient estimate (TE) method calculates the ratio:

$$E_{TE}(t) = \frac{\int \Psi \mathcal{H} e^{-t(H-E_T)}\Psi}{\int \Psi \exp[-t(\mathcal{H}-E_T)]\Psi} \tag{32}$$

Clearly the variational theorem applies: $E_{TE}(t) \geq E_0$. Also the energy converges exponentially fast in t:

$$\lim_{t\to\infty} E_{TE}(t) = E_0 + O(e^{-tE_g}) \tag{33}$$

where E_g is the gap to the next excited state with the same quantum numbers as the fermion ground state. In a Fermi liquid this is the gap to the state with the same momentum, parity and spin and would be obtained by making 2 particle-hole excitations.

For a method to self-consistently find its own nodes, the walks must be able to go anywhere, and so the drift term in eq. (27) must not diverge at the nodes. Hence we must distinguish between the antisymmetric trial function that is used to calculate the energy, $\Psi(R)$, (this is always assumed to be our best variational function) and a strictly positive guide function, $\Psi_G(R)$, used to guide the walks. The guide function appears in the drift and branching terms of eq. (27) and will be assumed to be a reasonable boson ground state trial function while the trial function appears in eq. (32). The Ψ_G importance-sampled Green's function is:

$$\tilde{G}(R,R';t) = \Psi_G(R) < R|e^{-t(\mathcal{H}-E_T)}|R' > \Psi_G^{-1}(R'), \tag{34}$$

and we can rewrite eq. (32) as:

$$E_{TE}(t) = \frac{\int \sigma(R)E_{LT}(R)\tilde{G}(R,R';t)\sigma(R')\Psi_G^2(R')}{\int \sigma(R)\tilde{G}(R,R';t)\sigma(R')\Psi_G^2(R')} \tag{35}$$

where $\sigma(R) = \Psi(R)/\Psi_G(R)$ and $E_{LT}(R)$ is the local energy of Ψ. In the limit, $\Psi_G \to |\Psi|$, σ equals the sign of the trial function.

The transient estimate algorithm is:

1. Sample configuration R' from the square of the guide function with VMC. That corresponds to the rightmost factor in the above integrands.
2. Record the initial sign of the walk, $\sigma(R')$.
3. Propagate the walk forward an amount of time, t with the Green's function, $\tilde{G}(R,R';t)$. If a branch occurs, each branch will count separately.
4. The weight of the walk arriving at R is $\sigma(R)\sigma(R')$. The energy at time t is computed as:

$$E_{TE}(t) = \frac{< [E_{LT}(R) + E_{LT}(R')]\sigma(R)\sigma(R') >}{< \sigma(R)\sigma(R') >}, \tag{36}$$

where the averages are over all random walks generated by this process.

The weight of the walk is positive if the walk crosses an even number of nodes (or does not cross at all) and is negative if it crosses once or an odd number of times. The trial function nodes are displaced by an unequal diffusion of walks from one side or the other.

The release node (RN) algorithm[27, 29] is an improvement on this TE method. Instead of projecting from the trial function, one begins the projection from the fixed-node solution. There are several advantages. First of all boson correlation within the fixed-nodes is already optimized, thus the projection time is only determined by the time to adjust the position of the nodes (of course this will indirectly affect the bosonic correlation). Second, one can directly calculate the difference between the exact result

and the fixed-node solution. It turns out that this is given by the local energy of walks as they cross the nodes. Thus the difference is obtained with more statistical accuracy than either energy alone which allows the convergence to be carefully monitored. Finally the release node method can be conveniently integrated into a fixed-node program. The only modifications are to introduce a guide function, and to keep track of the energy as a function of time since nodal crossing. The Ceperley-Alser results[26] for the 3DEG were done with the RN method. For complex trial function one can perform released phase simulation[48], a straightforward generalization of release node.

However there are serious problems with both the TE and RN method. Let us examine how the statistical error of the eq. (32) depends on the projection time. Note that the value of both the numerator and denominator are asymptotically proportional to $\exp(-t(E_F - E_T))$. Thus to keep the normalization fixed our trial energy must be equal to E_F. But because the guide function allows the walks to cross the nodes, the population will increase as $\exp(-t(E_B - E_T))$ where E_B is the boson energy. One can demonstrate that the signal-to-noise ratio vanishes exponentially fast. This is a general result. In any fermion scheme, as soon as negative weights are introduced the statistical error will grow as:

$$\epsilon_{stat} = e^{-t(E_F - E_B)}. \tag{37}$$

The behavior is physically easy to understand. Our estimator depends on finding differences between random walks crossing an even or an odd number of times. As soon as there is substantial mixing, the difference becomes harder and harder to see. Note that the exponential growth rate depends on a total energy difference. This implies that the transient estimate algorithm is guaranteed to fail if N is sufficiently large; the statistical errors will be too large. Nonetheless reliable results have been obtained for systems of 54 fermions.

The convergence problem is actually a bit more subtle since the projection time, t, can be chosen to give approximately equal statistical errors and systematic errors coming from non-convergence of the projection. Taking these errors from eqs. (33,37) we find the total error will decrease as:

$$\epsilon \propto P^{-\eta} \qquad \eta = \frac{E_g}{2(E_F - E_B + E_g)}. \tag{38}$$

where P is the total number of steps in the random walk. Only for bosons will $\eta = 1/2$. Any excited state will converge at a slower rate. Note that $\eta \propto 1/N$ for a fermion system. Inverting this relation, we find that the computer time needed to achieve a given error will increase exponentially with N.

There have been many attempts to "solve" the fermion sign problem. For example an obvious method is to try and pair positive and negative random walks in the TE method. This is difficult in many dimensions simply because the volume of phase space is so large than random walks rarely approach each other. There is some confusion about the nature of the "fermion" problem in the literature. Note that the TE and RN methods

do converge to the exact fermion energy. The fermion problem has to do with how long it takes to achieve a given error estimate, and, more precisely, how this scales with the number of fermions: the computational complexity of the calculation.

3˙5. *Problems with Projection methods.* – The projection method shares many of the same problems with the variational method. In fact, it is useful to think of the projection method as a "super-variational" method. In both the VMC and DMC methods there is a premium for good trial functions; that is the most straightforward way of making progress to solving the many-fermion problem. Our recent work[21] on finding more accurate analytic backflow-threebody shows that even for the well-studied homogeneous electron gas, significant improvements can still be made. Some general problems with projection methods:

- The fixed-node result is guaranteed to be closer to the exact answer than the starting variational trial function. Since the FN algorithm automatically includes bosonic correlation, the results are much less likely to have the human bias than with VMC. There is also the possibility of new things coming out of the simulation. For example, one may observe a particular type of correlation completely absent from the trial function. Hence, it is always good to pay close attention to correlation functions computed by DMC since that it is a good way of learning what is missing in the trial function. But it is slower than VMC because the time step needs to be smaller.

- Although the probability distribution does converge to the exact answer, in practice, this does not always occur in any given calculation of a many-body systems. The situation is similar to that of a classical simulation near a phase boundary. Metastable states exist and can have a very long lifetime. However, with DMC the importance sampling always biases the result. If the trial function describes a localized solid, even after complete convergence, the correlation functions will show solid-like behavior. Careful observation will reveal liquid-like fluctuations indicating the presence of the other state. The ability to perform simulations in a metastable state is useful but the results must be interpreted with caution.

- Importance sampling is only a partial cure to the unbounded fluctuations of the branching method. As N increases, sooner or later the branching becomes uncontrollable. Most projector Monte Carlo calculations have fewer than several hundred fermions. Finite temperature Metropolis methods do not suffer from the problem of uncontrolled branching. Also, as system gets larger, it becomes more important to monitor convergence, since necessary projection times can become larger. One is doing a simulation in 4D space-time and as the spatial length L is scaled, the length in Euclidean time β must be kept proportional.

- Although the fixed-node approximation dramatically improves energies, other properties, such as the momentum distribution, may not be improved. The projector methods can only calculate energies exactly. For all other properties one must

extrapolate out the effect of the importance sampling. This is a real problem if one is interested in obtaining asymptotic behavior of correlation functions. There are ways of getting around some of these problems such as forward walking, but none are totally satisfactory. The Path Integral finite temperature methods are superior to Projector Monte Carlo for calculating correlation functions. To explore the metal-insulator phase transition with FN-DMC, one must come up with a sequence of nodes spanning the transition and use the upper bound property of the fixed-node approximation. Reptation Monte Carlo[31] allows another way around this problem of mixed-estimators, though the scaling versus problem size is still an issue.

- Release node calculations only improve the nodes locally. If t is the release node projection time, then we can move the nodes a distance of at most $\sqrt{6N\lambda t}$. For this reason, it is important to build in exact long-range nodal properties.

4. – Ground state properties of the electron gas in 2 and 3 D

Here I will briefly summarize some of the results coming from the use of variational and diffusion Quantum Monte Carlo methods for the electron gas. In the 3DEG the Wigner Crystal transition was estimated within VMC[11] as $r_s = 67$. This was improved using DMC, both with fixed-node and released node algorithms and estimated the Wigner transition[26] at $r_s \approx 100 \pm 20$ and a polarized liquid state stable for $75 < r_s < 100$. Calculations of Ortiz[22] found a lower value for Wigner crystallization of $r_s = 65 \pm 10$ close to the older VMC results, in addition to a higher density spin-polarized phase starting at $r_s = 25 \pm 5$. Recent improved backflow calculations do not support these values. More accurate crystal calculations[32] estimate the melting transition at $r_s = 106 \pm 1$ and the spin polarization transition[30] at $r_s = 50 \pm 2$. Melting of the bosonic Wigner crystal at non-zero temperature has been studied using Path Integral Monte Carlo[47] finding an abrupt transition between classical thermal melting and quantum mechanical pressure melting.

Concerning the energies, a major improvement in the fluid phase was the introduction of backflow functions[19]. Twist averaging and analytic backflow[21] in the last few years has improved accuracy by potentially by an order of magnitude. We anticipate having much more accurate energies for the electron gas in the next few years.

Correlation energy, structure factor, radial distribution function, and momentum distribution of the spin-polarized uniform electron gas are tabulated in ref. [33]. Analytic static structure factors and pair-correlation functions obtained by fitting the QMC results and exact analytical limits for the unpolarized homogeneous electron gas including spin-resolved (up-up and up-down) correlation holes and static structure factors (unpolarized, for the range $0.8 < rs < 10$ are tabulated in ref. [34]. Quantum Monte Carlo calculations of the energy of the relativistic electron gas are considered in ref. [35]. A recent paper[36] considered the usual properties of the kinetic energy of the electron gas at finite temperatures. This followed observations reported in a restricted PIMC

calculations of the electron fluid[37].

For the 2DEG, the original VMC calculation found Wigner Crystallization[11] at $r_s = 33$ with a spin polarized state stable for $13 < r_s < 33$. This was followed up by a more accurate DMC study [38] resulting in an estimated transition at $r_s = 37 \pm 5$. Backflow trial functions were introduced[18]. There have been more recent DMC studies of the transition region and spin polarization[72, 74] with the conclusion that the spin polarized state may be stable between $26 \leq r_s 35$ though the energy differences are smaller than the systematic errors. We discuss next the calculation of Fermi liquid parameters in the 2DEG. Further studies of the correlation energy and spin polarization in the 2D electron gas are reported in ref. [39].

4˙1. *Fermi liquid parameters.* – Now I briefly sketch the calculation of the energy of particle-hole excitations. We calculated the ground state and the lowest particle-hole excitations of the system[20] using correlated sampling techniques similar to that used in optimizing the trial wavefunction. The ground state consists of filled shells of the wave vectors allowed by periodic boundary conditions. To calculate the fermi liquid parameters, we consider excited states which are generated by exciting a single electron from the last occupied shell of the ground state to the first unoccupied shell (see Fig. 1 of Ref. [20]). Because these states have different total momentum, they will be orthogonal. Two different excitations, spin-parallel excitations and spin-antiparallel ones, are possible. It is efficient to use a guiding or sampling function of the form:

$$\Psi_G^2(\mathbf{R}) \;=\; a_0\,\Psi_0^2(\mathbf{R}) \;+\; \sum_\alpha |\Psi_\alpha(\mathbf{R})|^2\,, \tag{39}$$

where Ψ_0 is the trial function for the ground state, Ψ_α for excited state α. The constant a_0 is set to be roughly equal to the number of excitations considered. This guiding function is non-negative and zero only where all states under consideration have zeroes. One then uses a single very long random walk to calculate the energies $E_o, \{E_\alpha\}$ using the reweighting method discussed earlier. Then the energy differences will have a much smaller error, than do the individual energies. See ref. [20] for details.

Following Fermi liquid theory analysis, the energy difference between two excited states α and β is given by

$$\Delta E_{\alpha\beta} \;=\; \sum_{l=1} (f_l^s \pm f_l^a)\,[-\cos(l\theta_\alpha) + \cos(l\theta_\beta)]\,, \tag{40}$$

where $\theta_{\alpha(\beta)}$ is the angle between particle momentum $\mathbf{k}_p$ and hole momentum $\mathbf{k}_h$ in excitation $\alpha(\beta)$ and the $+(-)$ sign corresponds to parallel (antiparallel) spins between particle and hole. The effective mass is determined by the first-order spin-symmetric component f_1^s:

$$\frac{m^*}{m} \;=\; (1 - \frac{1}{4} r_s^2 N f_1^s)^{-1}\,. \tag{41}$$

The f_1^s can be obtained by

$$Nf_1^s = \frac{N\Delta E_{14}^{\uparrow\uparrow} + N\Delta E_{14}^{\uparrow\downarrow}}{2(-\cos\theta_1 + \cos\theta_4)}, \tag{42}$$

where $\Delta E_{14}^{\uparrow\uparrow(\uparrow\downarrow)}$ is the energy difference between spin-parallel (-antiparallel) excitations 1 and 4. See ref. [20]for results.

4˙2. *Polarization of electron gas.* – In this section we discuss recent calculations of the polarization of the electron gas[30]. Despite years of active research, the properties of thermodynamic phases of the electron gas are not resolved experimentally or theoretically at intermediate densities. There has been recent interest in the low density phases spurred by the observation of a ferromagnetic state in calcium hexaboride (CaB_6) doped with lanthium[40]. The magnetic moment corresponds to roughly 10% of the doping density. The temperatures (600K) and densities ($7 \times 10^{19}/cm^3$) of this transition are in rough agreement with the predicted transition in the homogeneous electron gas.[22]. However, to make a detailed comparison, it is necessary to correct for band effects. For example, conduction electrons are located at the X-point of the cubic band structure and thus have a six-fold degeneracy. The effective mass of electrons at this point and the dielectric constant are also changed significantly from their vacuum values. These effects cast doubt on the viability of the electron gas model to explain the observed phenomena. Instead, excitonic and other models have been proposed to explain the ferromagnetism.

Considering now the spin degrees of freedom, at small r_s, electrons fill the Fermi sea with equal number of up spin and down spin electrons to minimize the total kinetic energy and thus the total energy; the system is in the paramagnetic state. As the density decreases and before the freezing transition, there is a possibility that the electrons become partially or totally polarized (ferromagnetic). The spin polarization is defined as $\zeta = |N_\uparrow - N_\downarrow|/N$, where $N_\uparrow$ and $N_\downarrow$ are the number of up and down spin electrons, respectively and $N = N_\uparrow + N_\downarrow$. For paramagnetic phase $\zeta = 0$ and for ferromagnetic phase $\zeta = 1$.

This polarization transition was suggested by Bloch[41] who studied the polarized electronic state within the Hartree-Fock (HF) approximation. He found the ferromagnetic state favored over paramagnetic state for $r_s > 5.45$, almost within the density of electrons in metals. However, HF is not reliable for $r_s > 0$.

Ceperley[11] using VMC with a Slater-Jastrow trial function determined that the transition between the polarized and unpolarized phase occurred at $r_s = 26 \pm 5$. Using DMC[26] it was estimated that the polarized fluid phase is stable at $r_s = 75 \pm 5$. An extension to this work[42] found the $\zeta = 0.5$ partially polarized fluid becomes stable at roughly $r_s \approx 20$ and the completely polarized state never stable. More recently Ortiz et al.[22] applied similar methods[22] to much larger systems ($N \leq 1930$) in order to reduce the finite-size error. They concluded the transition from the paramagnetic to ferromagnetic transition is a continuous transition, occurring over the density range of $20 \pm 5 \leq r_s \leq 40 \pm 5$, with a fully polarized state at $r_s \geq 40$.

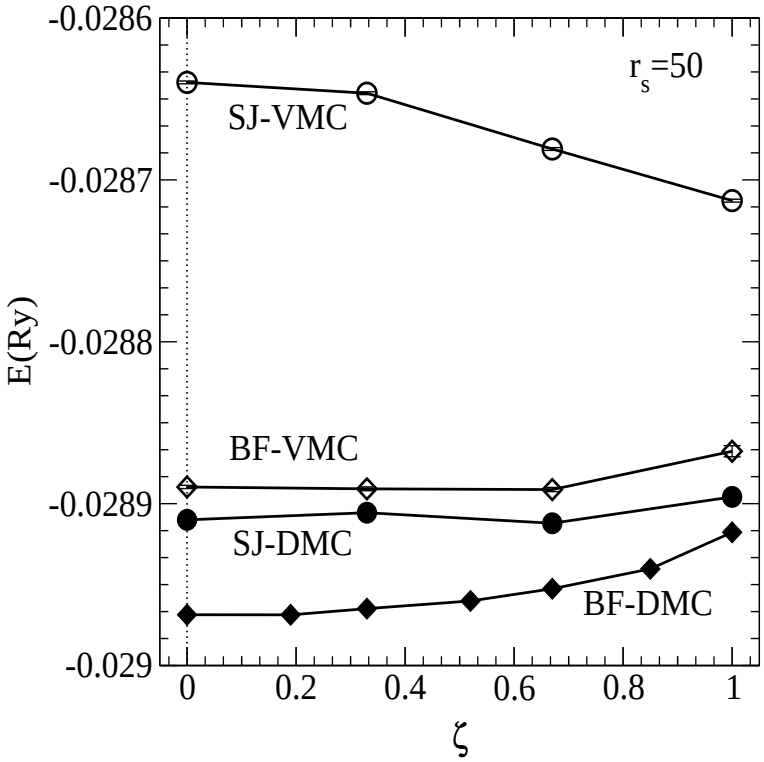

Fig. 4. – Energy versus spin polarization at $r_s = 50$ for 54 electrons using TA with 10^3 twist values. Compared are calculations with SJ and BF-3B wavefunctions and with two QMC methods: VMC and DMC.

Due to the very small energy differences between states with different polarizations, systematic errors greatly affect the QMC results, accurate trial wavefunctions are crucial to compute the small energy differences between different polarization states. Figure **4**˙2 shows the energy vs. polarization at $r_s = 50$ using different trial functions and simulation methods. The SJ trial function with VMC has the highest energy for all polarizations and at this level of accuracy finds the fully polarized phase to be stable, in agreement with earlier VMC calculations.[11] However, using the best BF-3B trial function, the variational energies are lowered significantly with the unpolarized energy dropping more than the polarized case so that the polarized phase is no longer stable. DMC calculations confirm this result. Note that the DMC energies determined using the NI phases (or nodes) give energies lower than the BF-3B variational energies confirming the importance of accurate DMC calculations. The use of BF-3B wavefunctions with DMC leads to the lowest ground state energies, hopefully, very close to the exact energy. Twist averaging is particularly advantageous for polarization calculations since shell effects dominate the polarization energy.

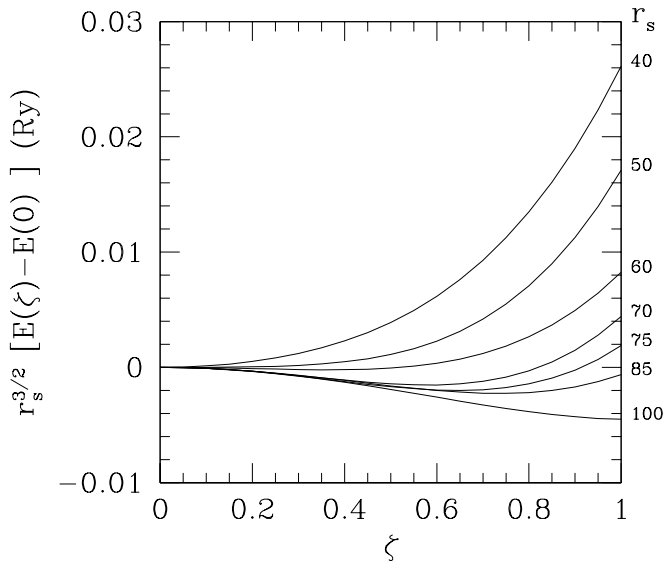

Fig. 5. – The spin polarization energy of the 3DEG times $r_s^{3/2}$ in Ry/electron at various densities using a cubic polynomial fit to the QMC data. The density, r_s, is denoted on the right axis.

The results are shown in figure 5. A polarization transition is evident. At $r_s = 40$, the system is still paramagnetic, with the unpolarized phase stable. As the density decreases, at $r_s \approx 50$, the system becomes unstable with respect to spin fluctuations. The partially polarized states become stable at $r_s \geq 60$. As the electronic density continues to decrease, the fully polarized state has a lower energy with respect to unpolarized state at $r_s \geq 80$, however, we find that the partially polarized state has an even lower energy.

In Fig. 6 is shown the predicted square of the optimal polarization versus density. It is found that the equilibrium polarization is described by $\zeta^2 = (r_s - r_s^*)/62$ with the critical density $r_s^* = 50 \pm 2$. As the density decreases, the stable state becomes more and more polarized, approaching fully polarized at freezing, $r_s \approx 100$. Quantum critical fluctuations, not present in systems with $N \leq 162$, could modify the behavior of the spin polarization energy near the critical density.

The quoted error bar on the critical density estimates the statistical errors, not the systematic errors arising from the fixed-phase approximation. The experimental and theoretical results on polarized helium give caution on placing too much confidence in the estimate of the polarization transition. Even using the accurate optimized BF-3B

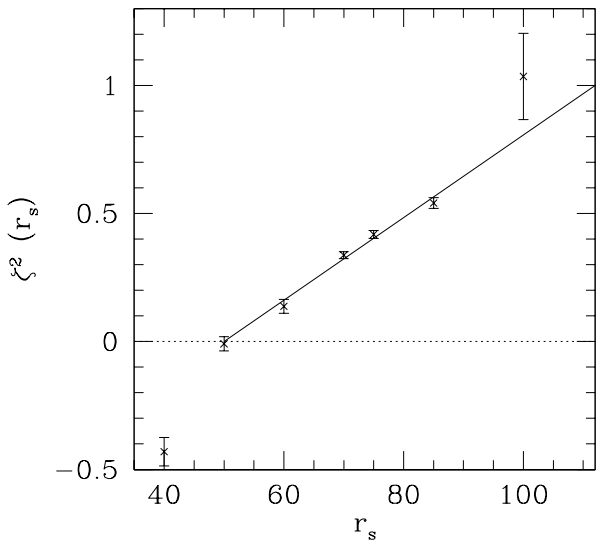

Fig. 6. – The square of the spin polarization versus r_s. The curves were obtained using fits in the Fig. (4). The line is a fit though the points. The value at $r_s = 40$ was obtained by extrapolation from physical values of ζ.

wavefunctions, the magnetic susceptibility in liquid ^{3}He does not agree with experiment at low pressure and the polarized phase is nearly degenerate with the unpolarized phase at the freezing density.[75] The present results also do not preclude the existence of phases with other order parameters such as superfluids, as occurs in ground state of liquid ^{3}He. In fact, it is rather likely that the ground state of the electron gas will have such a phase at the lowest fluid densities.

One can use the calculated energies to estimate the finite temperature behavior within the Stoner model[44] arising in the theory of itinerant magnetism[45]. The Stoner model differs from HF by replacing the Coulomb interaction by a zero range one, a repulsive delta function potential: $\sum_{i<j} g\delta(r_{ij})$. One can view this approach as the first step to a full Fermi-liquid description of the quasiparticle interactions, and use the QMC data to determine the strength of those interactions. One expects that the bosonic correlations have screened off the long-ranged interaction, leaving only a short-ranged spin-dependent term that can be modelled by a contact interaction.

In the Stoner model, the energy is evaluated within the mean field approximation.

The energy at zero temperature in the thermodynamic limit is:

$$E \propto (1+\zeta)^{5/3} + (1-\zeta)^{5/3} + 0.054 g r_s^2 (1-\zeta^2). \tag{43}$$

For $gr_s^2 < 20.5$ the system has an unpolarized ground state and for $gr_s^2 > 24.4$ the ground state is ferromagnetic. For intermediate couplings, the ground state has a partial spin polarization at zero temperature, similar to the observed behavior of the electron gas at low density.

Although the polarizations are qualitatively correct, the above functional form does not fit well the DMC data. In addition, assuming g does not have a very strong density dependence, the Stoner model predicts that the partially polarized density range should be quite narrow, from $50 \le r_s \le 54$, while as the QMC results indicate a much broader density range. Certainly, the assumption of a zero-range interaction of quasiparticles is too restrictive. However, we note that in the case of the 3D Ising model, the mean field estimate of the critical temperature is approximately 20% greater than the exact value, suggesting that the Stoner model will give a reasonable estimate of the transition temperature if the effective couplings are determined from the QMC ground state energies.

We use the Stoner model to make a estimate of the transition temperature of the polarized phase as follows. The free energy[46] in a fixed volume V in the Stoner model is:

$$F = F_0(N_\downarrow) + F_0(N_\uparrow) + \frac{g N_\uparrow N_\downarrow}{V}. \tag{44}$$

For large N the free particle free energy is:

$$F_0(N) = N\mu - k_B T \sum_k \ln(1 + e^{-\beta(e_k - \mu)}). \tag{45}$$

The chemical potential μ of each spin species is determined by the number of particles with that spin.

Fig. 7 is the estimated phase diagram of the 3D electron gas. Note that both the temperatures and densities of our calculated magnetic transition are four orders of magnitude smaller than that found experimentally[40] in CaB_6. Even assuming errors because of uncertainties in material properties and systematic errors in the calculation of T_c, these estimates are very difficult to reconcile with experiment, apparently ruling out an electron gas model of ferromagnetism in this material. An estimate of the limit of stability of the Wigner crystal [47] is also shown.

There is recent work on the low density electron gas in 2D, studying both the Fermi liquid[39] and the Wigner crystal phase. Using QMC similar techniques in the liquid phase, a polarized phase is found to be stable between $26 \le r_s \le 35$, though the energy differences are even smaller than in 3D. The partially polarized phase is never stable. In the 2D Wigner crystal, path integral methods[49] were used to derive directly the spin Hamiltonian. It was found that the ground magnetic state is a spin liquid though

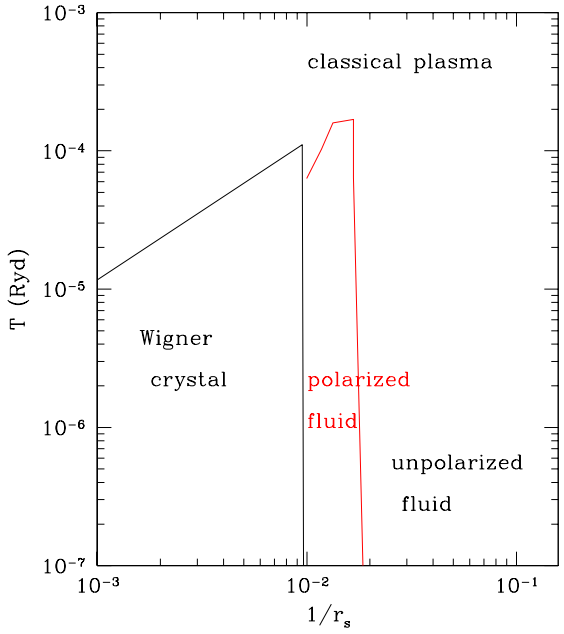

Fig. 7. – The predicted phase diagram of the 3DEG from QMC calculations. The solid line the mean-field estimate of the magnetic transition temperature from the Stoner model, where the spin interaction is estimated from the zero temperature QMC data. The dotted line is the energy difference between the unpolarized and partially polarized system.

the ferromagnetic state has only a slightly higher energy at melting. We will discuss this below. Analogous calculations of the magnetic phase diagram of the WC in 3D are underway[50].

4˙3. *Calculation of spin and charge response.* – The majority of QMC calculations have been for equilibrium properties such as energy, one-particle-orbital occupation numbers, and static correlation functions. Here I briefly discuss the basis of calculations of the spin and charged response[52, 53]. Apart from their intrinsic interest, these response functions are of importance to density functional developments beyond LDA[54, 55].

The static density-density response function is directly calculable by QMC. Rather than evaluate it in terms of the fluctuation-dissipation theorem, we use the definition of static response function by applying a static external potential:

$$v_{ext}(\mathbf{r}) = 2v_{\mathbf{q}} cos(\mathbf{q} \cdot \mathbf{r}), \tag{46}$$

which induces a modulation of the density with respect to its mean value, n_0. Such a modulation contains periodic components at all wavevectors that are non-vanishing integer multiples of $\mathbf{q}$. In particular, one finds a modulation with wavevector $\mathbf{q}$, $n_1(r) = 2n_{\mathbf{q}}cos(\mathbf{q}\cdot\mathbf{r})$, where

$$n_{\mathbf{q}} = \chi(q)v_{\mathbf{q}} + C_3 v_{\mathbf{q}}^3 + \cdots, \tag{47}$$

only contains odd powers of $v_{\mathbf{q}}$. Here $\chi(q)$ denotes the static density-density linear response function in Fourier space. Similarly the ground state energy (per particle) can be expanded in even powers of $v_{\mathbf{q}}$:

$$E_v = E_0 + \frac{\chi(q)}{n_0} v_{\mathbf{q}}^2 + C_4 v_{\mathbf{q}}^4 + \cdots. \tag{48}$$

The coefficients C_3 and C_4 in the above equations are determined by the cubic response function. QMC allows the direct evaluation of both $n_{\mathbf{q}}$ and E_v, for given $\mathbf{q}$ and $v_{\mathbf{q}}$. One performs simulations at few coupling strengths $v_{\mathbf{q}}$ and then extract $\chi(q)$ as well as the higher order response functions from the calculated $n_{\mathbf{q}}$ or E_v, by fitting in powers of $v_{\mathbf{q}}$.

There are several possibilities for the trial function in the external field. The first form is:

$$\Psi_T^v(\mathbf{R}) = \Psi_T^0(\mathbf{R}) \prod_i exp[\alpha cos(\mathbf{q}\cdot\mathbf{r}_i)], \tag{49}$$

with α a new variational parameter, related to the external potential strength $v_{\mathbf{q}}$. One can easily show that $\Psi_T^v(\mathbf{R})$, to leading order in α, correctly yields $n(\mathbf{r}) = n_0 + 2\alpha\gamma cos(\mathbf{q}\cdot\mathbf{r})$, with γ a function of the density n_0. To determine the relationship between the amplitude of the external potential $v_{\mathbf{q}}$, and the variational wavefunction parameter α, it is convenient to fix the wavefunction parameter α and determine the corresponding potential $v_{\mathbf{q}}$ which satisfies the minimum condition $\partial E_v/\partial\alpha = 0$. Once the trial function Ψ_T has been optimized, DMC is used to evaluate the total energy and the Fourier component $n_{\mathbf{q}}$ of the density. One should keep in mind that while the estimate of the energy is exact, within statistical errors, the *extrapolated estimate*[15] yielding $n_{\mathbf{q}}$ is approximate. In fact its accuracy depends quadratically on the difference $\delta\Psi \equiv \Psi_0 - \Psi_T$. Therefore, it is better to evaluate $\chi(q)$ from the energy, using Eq.(48).

Although the nodal structure of Φ_T^0 is thought to be accurate enough for the unperturbed system, the nodes of the trial function discussed above do not depend on the perturbation; one knows is incorrect for non-interacting particles. A second trial function

$$\Phi_{T,2}^v = D_\uparrow^v D_\downarrow^v e^{-U}, \tag{50}$$

is obtained by constructing the determinants D_s^v in terms of one-particle orbitals (Mathieu functions) for non-interacting electrons in a new external field, $v'(\mathbf{r}) = \alpha cos(\mathbf{q}\cdot\mathbf{r})$, with α a variational parameter. In general, $\Phi_{T,2}^v$ will possess a different nodal structure

, while still yielding a modulated density. It is found that the energy of this second trial function is lower. Note that the effective potential should be weak enough that the filling of the single particle orbitals is not altered.

This method of evaluating the static response functions is computationally demanding: to obtain $\chi(q)$, at a given thermodynamic state, requires a few simulations for each wavevector q—thus involving of the order of tens of simulations to construct $\chi(q)$ over the range of relevant wavevectors. Though the use of the fluctuation-dissipation theorem could in principle require less computer time, since the entire response function would be calculated at once, estimation of the systematic errors for the convergence of the time integral are problematical and the formula is not appropriate with fixed-node DMC. See refs. [52, 53] for details and results of calculations of the response functions.

5. – Path Integral Monte Carlo and Applications

Up to this point we have considered zero temperature methods, variational Monte Carlo and Diffusion Monte Carlo. Path Integrals have some significant advantages over zero temperature methods, as well as disadvantages, of course. Among the advantages is the absence of a trial wavefunction which means that quantum expectation values, including ones not involving the energy, can be directly computed. For the expert, the lack of an importance function may seem a disadvantage; without it one cannot push the simulation in a preferred direction. However, as the quantum system becomes more complex, it becomes increasingly difficult to devise satisfactory trial functions. It is my opinion that if quantum simulations are to attack the type of complex physical situations that classical simulations routinely deal with, it is better to have a formulation without a trial function. Only the Hamiltonian should enter. Of course, the explicit formulation at finite temperature also makes comparison with experiment more direct.

Thermodynamic properties are averages over the thermal N-body density matrix which is defined as a thermal occupation of the exact eigenstates $\phi_i(R)$:

$$\rho(R, R'; \beta) = \sum_i \phi_i^*(R) e^{-\beta E_i} \phi_i(R'). \tag{51}$$

The partition function is the trace of the density matrix.

$$Z(\beta) = e^{-\beta F} = \int dR \rho(R, R; \beta) = \sum_i e^{-\beta E_i} \tag{52}$$

Other thermodynamic averages are obtained as:

$$\langle \mathcal{O} \rangle = Z(\beta)^{-1} \int dR dR' \langle R|\mathcal{O}|R'\rangle \rho(R', R; \beta). \tag{53}$$

The density matrix can be calculated using path integrals. As first shown by Feynman (1953), the many-body density matrix can be obtained using classical-statistical methods

on polymer-like systems. The density matrix of a many-body system at a temperature $k_B T = \beta^{-1}$ can be written as an integral over all paths $\{R_t\}$:

$$\rho(R_0, R_\beta; \beta) = \frac{1}{N!} \sum_{\mathcal{P}} (\pm 1)^{\mathcal{P}} \oint_{\mathcal{P} R_0 \to R_\beta} dR_t \exp(-S[R_t]). \tag{54}$$

The path $R(t)$ begins at $\mathcal{P}R_0$ and ends at R_β, and $\mathcal{P}$ is a permutation of particle labels. For N particles, the path is in $3N$ dimensional space: $R_t = (\mathbf{r}_{1t}, \mathbf{r}_{2t} \ldots \mathbf{r}_{Nt})$. The upper sign is to be used for bosons and the lower sign for fermions. The *action* of the path, $S[R_t]$, is given by:

$$S[R_t] = \int_0^\beta dt \left[\frac{m}{2} \left| \frac{dR(t)}{\hbar dt} \right|^2 + V(R_t) \right]. \tag{55}$$

Thermodynamic properties, such as the energy, are related to the diagonal part of the density matrix, so that the path returns to its starting place or to a permutation $\mathcal{P}$ of its starting place after a "time" β.

Since the imaginary-time *action* $S[R_t]$ is a real function of the path, for boltzmannons and bosons the integrand is nonnegative. It can thus be interpreted as a probability of an equivalent classical system and the action as the classical potential energy of a "polymer." To perform Monte Carlo calculations of the integrand, one makes imaginary time discrete, so that one has a finite (and hopefully small) number of time slices and thus a classical system of N particles in M time slices; an equivalent NM particle classical system of "polymers." If the path integral is performed by a simulation method, such as a generalization of Metropolis Monte Carlo or with Molecular Dynamics, one can obtain essentially exact results for systems such as the properties of liquid ^{4}He at temperatures near the superfluid phase transition, the exchange frequency in quantum crystals, and quantum particles immersed in classical systems[61].

Note that in addition to sampling the path, the permutation is also sampled. This is equivalent to allowing the ring polymers to connect in different ways. This macroscopic "percolation" of the polymers is directly related to superfluidity as Feynman (1953) first showed. Any permutation can be broken into permutation cycles, *i. e.* into 2-, 3-, ... exchange cycles. Superfluid behavior can occur at low temperature when the probability of exchange cycles on the order of the system size is nonnegligible. For more details on the path integral theory of Bose superfluids and how one carries out the Monte Carlo calculations see[61].

However, the straightforward application of those techniques to Fermi systems means that odd permutations subtract from the integrand. This is the "fermion sign problem." Path integral methods as rigorous and successful as those for boson systems are not yet known for fermion systems in spite of the activities of many scientists throughout the last four decades.

Now let us consider how particle statistics are expressed in path integrals. For systems of identical particles, the states can be classified into symmetric and antisymmetric

states. The fermion density matrix is defined by restricting the sum to be only over antisymmetric states. (Similarly for other symmetries such as momentum or spin.) We shall denote the statistics of the particles by subscripts: ρ_F will denote the fermion density matrix, ρ_B the boson density matrix, ρ_D the boltzmannon (distinguishable particle) density matrix, and ρ any of the above density matrices.

For the moment, let us consider a single component system of spinless fermions. (By spinless fermions, we mean that the spatial wavefunction is antisymmetric with respect to interchange of all pairs of spatial variables.) Let $\mathcal{P}$ be one of the $N!$ permutations of particle labels. Using Eqs. (51) the density matrix has the following symmetries:

$$\begin{aligned} \rho(R,R';\beta) &= \rho(R',R;\beta) \\ \rho_F(R,R';\beta) &= (-1)^{\mathcal{P}}\rho_F(\mathcal{P}R,R';\beta) \\ \rho_F(R,R';\beta) &= (-1)^{\mathcal{P}}\rho_F(R,\mathcal{P}R';\beta). \end{aligned} \tag{56}$$

One can use the permutation (or relabeling) operator to construct the path integral expression for the boson or fermion density matrix in terms of the Boltzmann density matrix:

$$\rho_{B/F}(R,R';\beta) = \frac{1}{N!}\sum_{\mathcal{P}}(\pm 1)^{\mathcal{P}}\rho_D(\mathcal{P}R,R';\beta). \tag{57}$$

More generally, one uses some projection operator to select a desired set of states from the distinguishable particle density matrix which contains all states. From Eq. (56) we could (anti)symmetrize with respect to the first argument, the last argument or both. This connection between the boltzmannon density matrix and the Bose/Fermion density matrix is important because it is the boltzmannon density matrix that is built naturally from paths.

An alternative definition of the density matrix is by its evolution in imaginary time, the Bloch equation:

$$-\frac{\partial\rho(R,R';t)}{\partial t} = \mathcal{H}\rho(R,R';t) \tag{58}$$

which obeys the boundary condition at $t = 0$ for boltzmannon statistics:

$$\rho_D(R,R';0) = \delta(R-R') \tag{59}$$

or for Bose or Fermi statistics:

$$\rho_{B/F}(R,R';0) = \frac{1}{N!}\sum_{\mathcal{P}}(\pm 1)^{\mathcal{P}}\delta(\mathcal{P}R-R'). \tag{60}$$

The high temperature boundary condition is an (anti)symmetrized delta function.

Path integrals are constructed using the product property of density matrices:

$$\rho(R_0, R_2, \beta_1 + \beta_2) = \int dR_1 \rho(R_0, R_1; \beta_1)\rho(R_1, R_2; \beta_2). \tag{61}$$

The product property holds for any sort of density matrix.

If the product property is used M times we can relate the density matrix at a temperature β^{-1} to the density matrix at $M\beta^{-1}$:

$$\rho_{B/F}(R_0, R_M, \beta) = \frac{1}{N!}\sum_{\mathcal{P}}(\pm 1)^{\mathcal{P}} \int dR_1 \dots dR_{M-1} \rho_D(\mathcal{P}R_0, R_1; \tau) \dots \rho_D(R_{M-1}, R_M; \tau). \tag{62}$$

The sequence of intermediate points $\{R_1, R_2, \dots, R_{M-1}\}$ is the path, and the *time step* is $\tau = \beta/M$.

As the time step gets sufficiently small, we can write down an explicit expression for the density matrix ρ_D and thereby an explicit expression for $\rho(R_0, R_M; \beta)$, but one with lots of intermediate integrals and the permutational sum to perform. The Trotter theorem tells us that for sufficiently small τ we can assume that the kinetic and potential operators commute so that: $e^{-\tau\hat{\mathcal{H}}} = e^{\tau\mathcal{T}}e^{-\tau\mathcal{V}}$. Define the (boltzmannon) action as $S_D(R, R'; \tau) = -\ln[\rho_D(R, R'; \tau)]$. Then for small time step the action is:

$$S_D(R, R'; \tau) = \frac{3N}{2}\ln(4\pi\lambda\tau) + \frac{(R - R')^2}{4\lambda\tau} + \frac{1}{2}(V(R) + V(R')). \tag{63}$$

This is known as the *primitive approximation* to the action. The form of the action is analogous to the potential energy of classical "polymer" system with harmonic springs between neighboring beads and an interpolymer potential between different chains.

The boson action is real, but it is expressed as a sum over permutations. For large N it is not possible to evaluate directly the sum since it has $N!$ terms. It is better to leave the bosonic symmetrization as an explicit boundary condition on the paths and to sample the permutations as well as the paths. We will follow the same philosophy with restricted fermion paths, the reasons not being the difficulty of evaluating the resulting determinant (that is easier for fermions than for bosons) but to avoid the minus signs. For bosons or fermions we can (anti)symmetrize anywhere along the path as many times as we like. However relabeling is only necessary once. By convention we will just relabel the first step.

In the *direct fermion method* one sums over permutations just as for bosonic systems. Odd permutations then contribute with a negative weight. The direct method has a major problem because of the cancellation of positive and negative permutations as noted by Feynman and Hibbs (1965). It is possible to demonstrate that a distribution having both positive and negative regions will have an exponentially vanishing signal/noise ratio in a Monte Carlo calculation. At high temperatures

$$\xi = \exp[-2\rho N(2\pi\lambda\beta)^{3/2}]. \tag{64}$$

At the degeneracy temperature: $\xi \approx \exp(-N)$. The direct fermion method, while exact, becomes exceedingly inefficient as β and N increase, precisely when the physics becomes interesting.

The restricted path identity (or fixed-node) shows that the nodes of the exact density matrix determine the rule by which one can take only paths with the same sign; we can arrange things so that we only get positive contributions. We only use paths which do not cross the nodes of the fermion density matrix, and the results are identical to allowing all of the paths. Though the identity is exact, one faces precisely the same difficulty as in zero temperature methods: the nodal surfaces of the interacting fermion density matrix are unknown, so nodal surfaces coming from either perturbation theory, or the variational principle must be used. These methods lead to a very interesting description of fermion systems in terms of exchanging paths. However, we do not have space to describe them here and refer instead to the literature[57, 58]

5˙1. *Defects in the 2D Wigner Crystal.* – At sufficiently low densities, the ground state of a 2D electron gas is a Wigner crystal. In this section, I summarize the results of calculations of point-like defects in a clean 2D electron Wigner crystal[62]. The motivation for the study of defects is two-fold. First, localized defects are present in a finite concentration at any nonzero temperature (they have even been speculated to exist at zero temperature a super solid). Secondly, the melting process in 2D can be influenced or even determined by defect formation.

At large values of r_s, the exchange contributions to the energy are small as we discuss below, so one can assume distinguishable electrons and neglect antisymmetry but include it for $r_s \leq 75$. However, to keep the system stable, one must forbid particle exchange by enforcing the condition $|\mathbf{r}_i - \mathbf{s}_i| < 1.1a$ where a is the nearest neighbor distance and $\mathbf{s_i}$ is the i^{th} lattice site. Such a "tether" is realistic because in a quantum crystal exchanges are rare and the wave function is peaked around the lattice sites. One can also use restricted path integrals[57] to account for Fermi statistics. Only paths entirely in the positive region of the Slater determinant are allowed. Such a restriction is exact if the nodal surfaces of the trial density matrix are correct. For the nodes one can use a Slater determinant of Gaussian orbitals $\exp(-c(\mathbf{r}_i - \mathbf{s}_j)^2)$ with $\mathbf{s}_i$ the lattice sites and c taken from [11] with a ferromagnetic spin arrangement. Calculation of the tunnelling frequencies to determine the ground state magnetic ordering indicate that the magnetic energies are always much less than the defect energies[49] and that the system is nearly ferromagnetic in near melting. We find that the restriction also serves to stabilize the crystal against melting.

The energy to create $N_{\rm def}$ defects in a system with $N_l = N$ lattice sites is

$$\Delta E_{\rm def} = [e(N + N_{\rm def}) - e(N)]\,(N + N_{\rm def}), \tag{65}$$

where $e(n)$ is the energy per electron for a system containing n electrons with area $A = n/\rho$. This was evaluated with independent PIMC calculations with different number of particles rather than more efficient procedures where particles are inserted or removed.

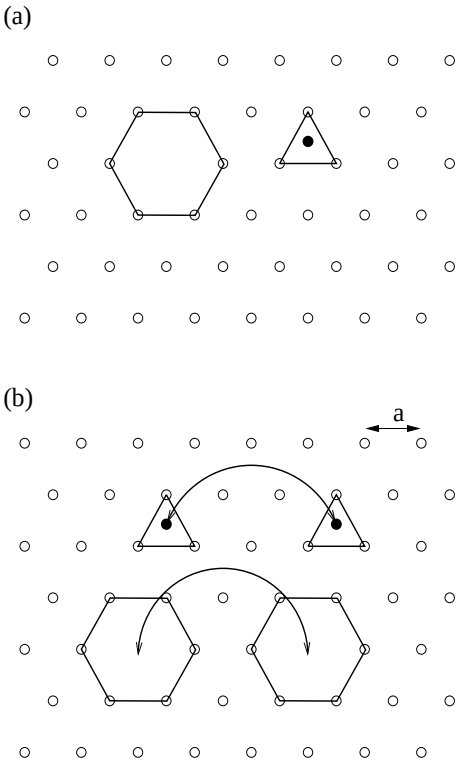

Fig. 8. – a) Hexagonal 2D Wigner crystal with a single 6-coordinated vacancy and a 3-fold coordinated centered interstitial (CI) defect. b) Pair vacancy and CI defects.

Such differential procedures are difficult because of the combination of large relaxation of the lattice, the very large zero point motion and the antisymmetry. The calculations are time-consuming as the system gets larger because one needs high accuracy to obtain the energy difference but the direct method allows better control over the systematic error.

Fig. 8 shows a vacancy and centered-interstitial (CI) defects in a 2D hexagonal lattice. Fig. 9 demonstrates that the formation energy for an interstitial is consistently lower than creation energy for vacancies in 2D Wigner crystals at all densities. For a Coulomb system without fermion exchange, the energy of a defect can be expanded as

$$E_D = c_1 r_s^{-1} + c_{3/2} r_s^{-3/2} + c_2 r_s^{-2} \ldots \tag{66}$$

The first term is the static potential energy of the defect, the second the harmonic energy of the defect. Cockayne and Elser[59] have done exact calculation of c_1 and $c_{3/2}$. Shown in the lower panel of Fig. 9 is the anharmonic contribution defined as the excess energy beyond the harmonic calculation. Anharmonic effects lower the defect energies to approximately half the harmonic value at $r_s = 50$. Cockayne and Elser find that the

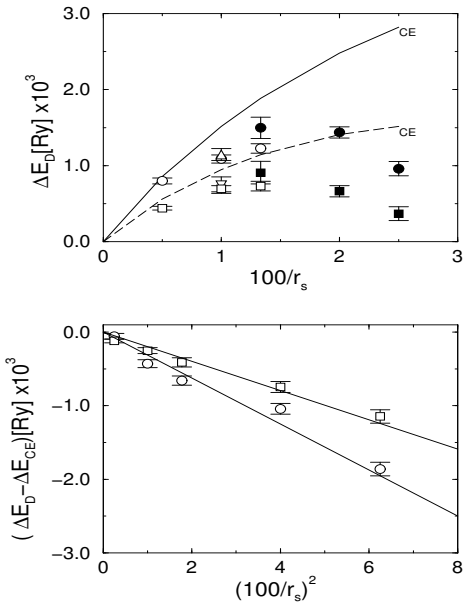

Fig. 9. – Formation energy (top figure) for vacancy (circle) and CI (square) defects as a function of $1/r_s$ at a temperature of 1.25×10^{-5}Ry for a system of 120 lattice sites (open and solid syimbols are for Boltzman and Fermi statistics respectively). The triangles are results with 340 lattice sites. The lines (solid for vacancy and dashed for interstitial) are from harmonic calculations[59]. The anharmonic energy is shown on the bottom panel.

defect energy vanishes for CI defects at $r_s = 15 \pm 1$ and $r_s = 9 \pm 1$ for vacancies. We estimate that E_D vanishes for interstitials at $r_s = 35 \pm 2$ and $r_s = 29 \pm 2$ for vacancies. The proximity of the vanishing of the interstitial creation energy to the melting density is highly suggestive that interstitial defects play a role in the melting process. The proliferation of vacancies for $r_s < 40$ could result in a continuous rather than first order quantum melting, analogous to what happens for the classical 2D Wigner crystal. It is possible that the assumption of the ferromagnetic spin arrangement has stabilized the crystal with respect to interstitials for $35 \leq r_s \leq 40$.

5˙2. *PIMC of exchange frequencies and magnetic ordering in the 2 wigner crystal.* – In this section I briefly review calculations[49] to determine the spin-spin interaction in the Wigner crystal, using Thouless'[63] theory of exchange. According to this theory, in the absence of point defects, at low temperatures the spins will be governed by a Hamiltonian of the form:

$$\mathcal{H}_{spin} = -\sum_P (-1)^P J_P \hat{\mathcal{P}}_{spin} \tag{67}$$

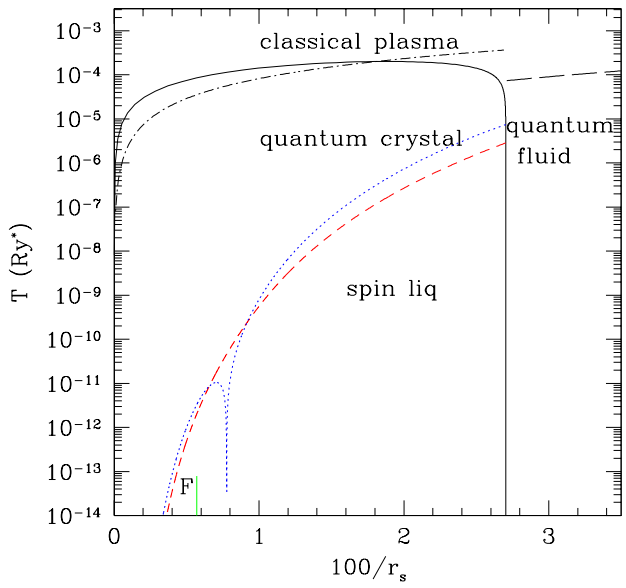

Fig. 10. – Phase diagram of the 2dEG. The estimated melting line is based on Lindemann's criteria. The long-dashed line represents the Debye temperature. The dotted line is the Curie-Weiss constant θ, the short dashed line is coefficient of the specific heat at high temperature, J_c as defined in the text. The vertical line is the estimated zero temperature ferromagnetic (F) transition.

where the sum is over all cyclic (ring) exchanges described by a cyclic permutation P, J_P is its exchange frequency and $\hat{\mathcal{P}}_{spin}$ is the corresponding spin exchange operator. Path Integral Monte Carlo (PIMC) as suggested by Thouless[63] and Roger[64] has proved to be the only reliable way to calculate these parameters. The theory and computational method have been tested thoroughly on the magnetic properties of bulk helium obtaining excellent agreement with measured properties[61]. Rather surprisingly, it has been found[65] that in both 2D and 3D solid ^{3}He, exchanges of 2, 3 and 4 particles have roughly the same order of magnitude and must all be taken into account. This is known as the multiple spin exchange model(MSE).

A WKB calculation of the exchange frequencies in the 2dWC by Roger[64] predicted that the three electron J_3 nearest neighbor exchange would dominate, leading to a ferromagnetic(F) ground state. Recent calculations[66, 67] have confirmed and extended those of Roger.

An exact method for calculating the exchange frequency in quantum crystals has been

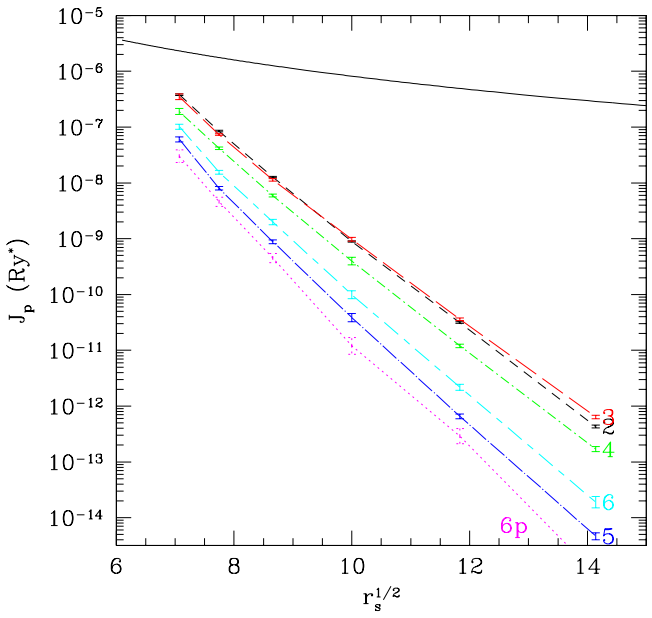

Fig. 11. – Exchange frequencies versus $r_s^{1/2}$. The solid line is 10^{-3} of the kinetic energy.

previously developed and applied to solid ^{3}He [68, 61, 69]. One computes the free energy necessary to make an exchange beginning with one arrangement of particles to lattice sites Z and ending on a permuted arrangement PZ:

$$F_P(\beta) = Q(P,\beta)/Q(I,\beta) = \tanh(J_P(\beta - \beta_0)). \tag{68}$$

Here $Q(P,\beta)$ is the partition function corresponding to an exchange P at a temperature $1/\beta$. I is the identity permutation. Note that these paths are of "distinguishable" particles since Fermi statistics are implemented through the spin Hamilitonian in Eq. (1). The function $F_P(\beta)$ is found with the Bennett method, which directly calculates free energy differences and thereby determines J_P and β_0.

The exchange frequencies vary rapidly with density as shown in fig. 11. One can see that they are much less than the zero point energy of the electrons, thus justifying the use of Thouless' theory. The WKB method[65], where one approximates the Path Integral in Eq. (2) by the single most probable path, explains most of this density dependence.

In the 2dWC, the WKB expression for the exchange frequency[64, 66, 67] is:

$$J_P = A_P(r_s) b_P^{1/2} r_s^{-5/4} e^{-b_P r_s^{1/2}}. \tag{69}$$

Here $b_P r_s^{1/2}$ is the minimum value of the action integral along the path connecting PZ with Z. The 3 particle exchange exponent is the smallest indicating that as $r_s \to \infty$, J_3 will dominate and the system will have a ferromagnetic ground state. However, note that in Fig. 11 $J_2 > J_3$ for $r_s \leq 90$.

Having determined the exchange frequency, one is left with the spin Hamiltonian of Eq. (1). This is a non-trivial many-body problem. For spin 1/2 systems, J_2 and J_3 contribute only with a nearest neighbor Heisenberg term: $J_2^{\text{eff}} = J_2 - 2J_3$. This term is negative (ferromagnetic) but approaches zero near melting. For convenience we use J_4 as a reference to fix the overall scale of the magnetic energy. Neglecting J_{6p}, the Hamiltonian has 3 remaining parameters J_2^{eff}/J_4, J_5/J_4 and J_{6h}/J_4. The dependence of these ratios on density is shown in fig. (5).

High temperature series expansions[70] determine the the specific heat C_V and magnetic susceptibility χ_0/χ for temperatures $k_B T \gg J_P$. The susceptibility is given by: $\chi_0/\chi = T - \theta + B/T \ldots$ and the specific heat $C_V/Nk_B = (3J_c/2T)^2 + \ldots$ where the Curie-Weiss constant is given by $\theta = -3(J_2^{\text{eff}} + 3J_4 - 5J_5 + 5/8 J_{6h} + 15/4 J_{6p})$ with a quadratic expression of the J's for J_c. These two constants, which set the scale of the temperature where exchange is important, are shown as a dotted and dashed lines on fig. (1). Note that θ changes from positive to negative at $r_s \approx 130$. Both θ and J_c decrease very rapidly at low density showing that experiments must be done at $r_s \leq 60$ if spin effects are to be at a reasonable temperature, e.g. $T_c > 0.1mK$ (assuming the values for Si-MOSFET: $\epsilon = 7.7, m^* = 0.2$).

The zero temperature state can be studied by exact diagonalization[71] (ED) of an N site system. (The present limitation is $N < 36$.) Two phases are important: the ferromagnetic (F) phase and an antiferromagnetic(AF) phase. The F-AF transition is shown in fig. 10. The ferromagnetic phase is obtained only at very low density: the transition for the 2dWC will occur at $r_s = 175 \pm 10$. At higher density, the frustration between large cyclic exchanges (4-6 body loops) results in a disordered spin state[71]. For example, at $r_s = 100$, is a spin liquid with a gap to all excitations. At higher densities ($r_s < 100$), the trajectory of the MSE models parallels the F-AF phase line, with the possibility of a re-entrant ferromagnetic phase for $r_s < 40$. Note that QMC calculations[72] of the normal fermi liquid at $r_s = 30$ show that the ferromagnetic phase has a slightly lower energy that the unpolarized phase. Hence both the high density 2dWC and the low density electron fluid are characterized by a spin Hamiltonian which is nearly ferromagnetic.

* * *

This work was supported by NSF DMR 01-04399 and the Department of Physics at the University of Illinois Urbana-Champaign. Many of the computations were performed with the facilities at the NCSA. This article summarizes a series of calculations and

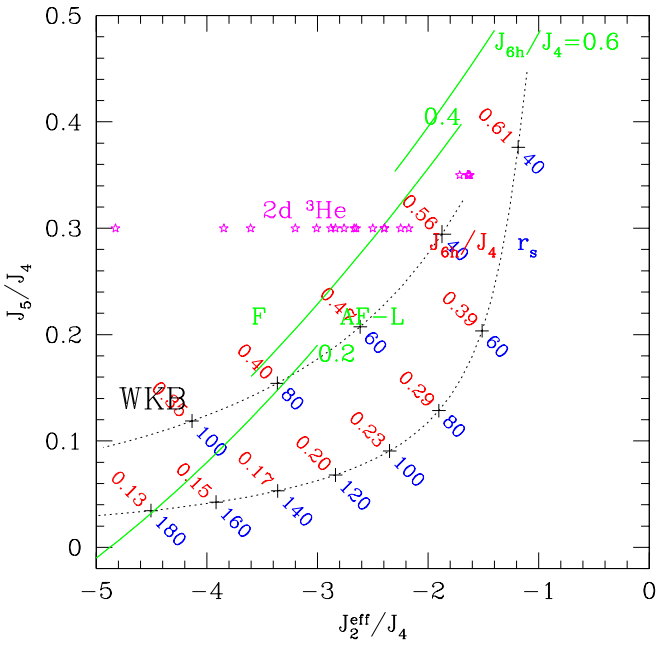

Fig. 12. – Spin Phase diagram of the 2DEG as a function of exchange ratios. The dotted line is the flow of spin hamiltonian space versus r_s (lower numbers); also shown the are estimated values of J_{6h}/J_4(upper numbers). The solid lines are the limit of the ferromagnetic phase according to ED[71] at $J_{6h}/J_4 = \{0.2, 0.4, 0.6\}$. The 2dWC crosses into the F region for $r_s \approx 175$. The ($\star$) are empirical estimates of the spin Hamiltonian of 2d ^{3}He at several densities[73].

papers with various coauthors through the years: B. J. Alder, E. L. Pollock, Y. K. Kwon, R. M. Martin, B. Bernu, L. Candido, P. Phillips, M. Holzmann, F.H. Zong, C. Lin, G. Senatore and S. Moroni.

REFERENCES

[1] E. Wigner, Phys. Rev. **46**, 1002 (1934).
[2] J. M Hammersley and D. C. Handscomb, *Monte Carlo Methods*, Chapman and Hall, 1964.
[3] W. M. C. Foulkes, L. Mitas, R. J. Needs and G. Rajagopal, Rev. Mod. Phys. **73** 33 (2001).
[4] N. Metropolis, A. W. Rosenbluth, M. N. Rosenbluth, A. H. Teller and E. Teller, J. Chem. Phys. 21, 1087(1953).
[5] M. H. Kalos and P. A. Whitlock *Monte Carlo Methods*, Wiley, 1986.
[6] W. L. McMillan, Phys. Rev. A 138, 442 (1965).
[7] D. M. Ceperley, G. V. Chester and M. H. Kalos Phys. Rev. B16,3081 (1977).

[8] R. Jastrow, Phys. Rev. 98, 1479 (1955).
[9] A. Bijl, Physica, 7, 869 (1940).
[10] D. Ceperley, J. of Stat. Phys. 43, 815 (1986).
[11] D. M. Ceperley, Phys. Rev. B18, 3126 (1978).
[12] T. Gaskell, Proc. Phys. Soc. London **77**, 1182 (1961).
[13] M. P. Allen and D. J. Tildesley, *Computer Simulation of Liquids*, Oxford, 1987.
[14] V. Natoli and D.M. Ceperley , J. Comp. Phys. **117**, 171 (1995).
[15] D. M. Ceperley and M. H. Kalos in *Monte Carlo Methods in Statistical Physics* ed. K. Binder, Springer-Verlag (1979).
[16] S. Vitiello and K. Runge and M. H. Kalos, Phys. Rev. Letts. **60**, 19701972" (1988).
[17] J.P. Bouchaud and C. Lhuillier, Europhys. Lett. 3, 1273(1987).
[18] Y. Kwon, D. M. Ceperley and R. M. Martin, Phys. Rev. B **48**, 12037 (1993)
[19] Y. Kwon, D. M. Ceperley and R. M. Martin, Phys. Rev. B **58**, 6800 (1998).
[20] Y. Kwon, D. M. Ceperley, and R. M. Martin, Phys. Rev. B50, 1684 (1994).
[21] M. Holzmann, D. M. Ceperley, C. Pierleoni and K. Esler, "Backflow Correlations for the Electron Gas and Metallic Hydrogen", Phys. Rev. E, **68**, 046707:1-15(2003).
[22] G. Ortiz, M. Harris and P. Ballone, Phys. Rev. Lett. **82**, 5317 (1999).
[23] C. Lin and F. H. Zong and D. M. Ceperley, Phys. Rev. E **64**, 016702 (2001).
[24] M. D. Donsker and M. Kac, J. Res. Natl. Bur. Stan. 44,551(1950).
[25] M. H. Kalos, D. Levesque and L. Verlet, Phys. Rev. A 9,2178 (1974).
[26] D. M. Ceperley and B. J. Alder Phys. Rev. Letts. 45, (1980).
[27] D. M. Ceperley, in *Recent Progress in Many-Body Theories*, ed. J. Zabolitzky, Springer-Verlag (1981).
[28] D. M. Ceperley, in J. Stat. Phys. 63, 1237 (1991).
[29] D. M. Ceperley and B. J. Alder, J. Chem. Phys. 81,5833 (1984).
[30] F. H. Zong, C. Lin and D. M. Ceperley, Phys. Rev. E 66, 036703(2002).
[31] S. Baroni, and Moroni, S., *Phys. Rev. Lett.*, **82**, 4745–4748 (1999).
[32] N. D. Drummond et al."Diffusion Quantum Monte Carlo study of 3D Wigner Crystals", preprint 2003.
[33] G. Ortiz and P. Ballone Phys. Rev. B 50, 1391-1405 (1994).
[34] P. Gori-Giorgi, F. Sacchetti and GB. Bachelet, Phys. Rev. B, **61**, 7353 (2000).
[35] S. D. Kenny, G. Rajagopal, R. J. Needs, W.-K. Leung, M. J. Godfrey, A. J. Williamson, and W. M. C. Foulkes, Phys. Rev. Lett. 77, 1099 (1996).
[36] B. Militzer and E. L. Pollock, Phys. Rev. Lett. 89, 280401 (2002).
[37] C. Pierleoni,B. Bernu, D. M. Ceperley and W. R. Magro, Phys. Rev. Lett. 73, 2145 (1994).
[38] B. Tanatar and D.M. Ceperley, Phys. Rev. B 39, 5005 (1989).
[39] C. Attaccalite, S. Moroni, P. Gori-Giorgi and G. Bachelet, Phys. Rev. Lett. 88, 256601 (2002).
[40] D. P. Young, Nature **397**, 386 (1999).
[41] F. Bloch, Zeit. Physik **57**, 545 (1929).
[42] B. J. Alder, D. M. Ceperley and E. L. Pollock, Int. J. of Qu. Chem. **16**, 49 (1982).
[43] G. Ortiz and D. M. Ceperley and R. M. Martin, Phys. Rev. Lett. **71**, 2777 (1993).
[44] E. Stoner, Proc. Roy. Soc. A **165**, 372 (1939); A **169**, 339 (1939).
[45] C. Herring, in *Magnetism*, vol **IV**, (eds. G. T. Rado and H. Suhl) (Academic Press, San Diego, 1966).
[46] R. A. Suris, Sov. Phys. Solid State **3**, 1303 (1961).
[47] M. D. Jones and D. M. Ceperley, Phys. Rev. Lett. **76**, 4572 (1996).
[48] M. D. Jones, G. Ortiz, and D. M. Ceperley, Phys. Rev. E 55 , 6202 (1997).
[49] B. Bernu, L. Candido and D. M. Ceperley, Phys. Rev. Lett. **86**, 870 (2001).
[50] L. Candido, D. M. Ceperley, and B. Bernu, work in progress (2003).

[51] P.J. Reynolds, D.M. Ceperley, B. J. Alder, and W.A. Lester, J. Chem. Phys. **77**, 5593 (1982).
[52] S. Moroni, D. M. Ceperley and G. Senatore, Phys. Rev. Lett. 69, 1837 (1992).
[53] S. Moroni, D. M. Ceperley and G. Senatore, Phys. Rev. Lett. 75, 689 (1995).
[54] P. Hohenberg and W. Kohn, Phys. Rev.**136**, B864, (1964); O. Gunnarson, M. Jonson, and B. I. Lundqvist, *ibid.* **B20**, 3136 (1978); S. Moroni and G. Senatore *ibid.* **B44**, 9864 (1991).
[55] G. Senatore and G. Pastore, Phys. Rev. Lett. **64**, 303 (1990); A. R. Denton, P.Nielaba, K. J. Runge, and N. W. Ashcroft, *ibid.* **64**, 1529 (1990).
[56] S. T. Chui and B. Tanatar, Phys. Rev. Lett. **74**, 458 (1995); A. G. Eguiluz, A. A. Maradudin, and R. J. Elliott, Phys. Rev. B **27**, 4933 (1983).
[57] D. M. Ceperley, Phys. Rev. Letts. **69**, 331 (1992).
[58] D. M. Ceperley, in Monte Carlo and Molecular Dynamics of Condensed Matter Systems, Ed. K. Binder and G. Ciccotti, Editrice Compositori, Bologna, Italy, 1996.
[59] E. Cockayne and V. Elser, Phys. Rev. B **43**, 623 (1991).
[60] E. L. Pollock and D. M. Ceperley. Phys. Rev. B, **30**, 2555 (1984).
[61] D. M. Ceperley, Rev. Mod. Phys. **67**, 279 (1995).
[62] L. Cândido, P. Phillips and D. M. Ceperley, Phys. Rev. Lett. 86, 492 (2001).
[63] D. J. Thouless, Proc. Phys. London **86**, 893 (1965).
[64] M. Roger, Phys. Rev. B **30**, 6432 (1984).
[65] M. Roger, J. H. Hetherington and J. M. Delrieu, Rev. Mod. Phys. **55**, 1 (1983).
[66] S. Chakravarty, S. Kivelson, C. Nayak and K. Voelker, Phil. Mag. B **79**, 859 (1999). (cond-mat/9805383).
[67] M. Katano and D. S. Hirashima, Phys. Rev. B **62**, 2573 (2000).
[68] D. M. Ceperley and G. Jacucci, Phys. Rev. Letts. **58**, 1648 (1987).
[69] B. Bernu and D. Ceperley in *Quantum Monte Carlo Methods in Physics and Chemistry*, eds. M.P. Nightingale and C.J. Umrigar, Kluwer (1999).
[70] M. Roger, Phys. Rev. B **56**, R2928 (1997).
[71] G. Misguich, B. Bernu, C. Lhuillier and C. Waldtmann, Phys. Rev. Letts. **81**, 1098 (1998); Phys. Rev. B **60**, 1064 (1999).
[72] D. Varsano, S. Moroni and G. Senatore, Europhys. Lett. 53, 348 (2001).
[73] M. Roger, C. Bauerle, Yu. M. Bunke, A.-S. Chen and H. Godfrin, Phys. Rev. Letts. **80**, 1308 (1998).
[74] F. Rapisarda and G. Senatore, Aust. J. Phys. **49**, 161 (1996); Int. J. Mod. Phys. B **13**, 479 (1999).
[75] F. H. Zong, D. M. Ceperley, S. Moroni, and S. Fantoni, Mol. Phys. 101, 1705 (2003).